Coupling dynamics of membrane bending proteins for COPII vesicle formation

Master thesis

Written by *Louise Krogsgaard Madsen*

May 20th 2021

Supervised by
Ala Trusina

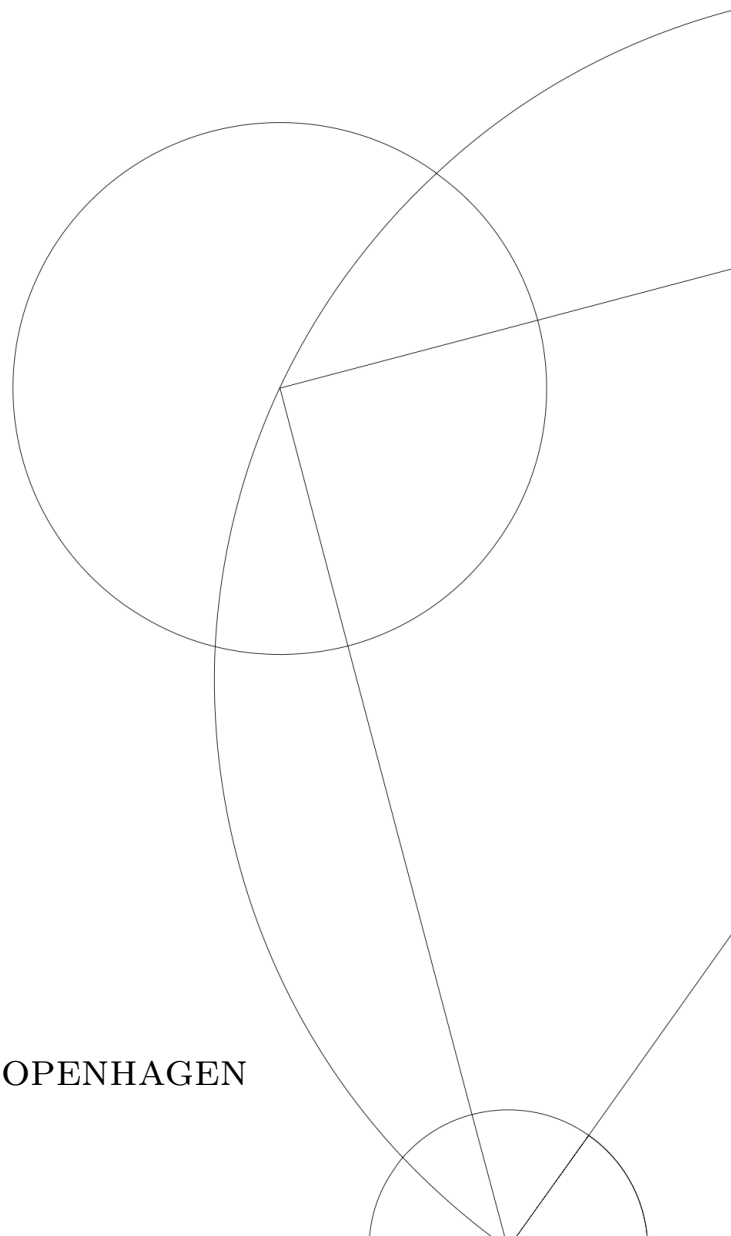

University of Copenhagen

UNIVERSITY OF COPENHAGEN

Name of Institute:	Niels Bohr Institute
Name of Department:	Biocomplexity and Biophysics
Author(s):	Louise Krogsgaard Madsen
Email:	louisekrogsgaard@tutanota.com
Title and subtitle:	Coupling dynamics of membrane bending proteins for COPII vesicle formation -
Supervisor(s):	Ala Trusina
Handed in:	20.5.2021
Defended:	

Name _____

Signature _____

Date _____

Abstract

The majority of proteins translated at the Endoplasmic Reituculum (ER) leave the ER through a COPII vesicle before they continue along their secretory pathway.

By understanding the COPII formation better, diseases related to the formation can be better understood. It is also possible that a working COPII vesicle formation can be inhibited in cancer cells to prevent them from spreading further.

The key proteins to control the formation process are called COPII proteins. Some of their interactions as well as their role in the process are still being debated. We investigate if a simple network of their interactions can reproduce vesicle formation. This is done by setting up a model of the COPII protein interactions and coupling this to a model of polarized interacting particles that emulates the ER membrane. There after we simulate how the membrane deforms during vesicle formation.

It is widely accepted that the key COPII protein, Sar1, initiates membrane bending [7], [28], [2], [6], [6], [25]. We succeed to form spherical vesicles that leave the membrane while assuming that Sar1 does not bend the membrane equally much in all directions in the membrane plane. With this assumption we also reproduced experimental results where a mutant of Sar1 makes tube formations.

The role of cargo is also still being discussed. Based on how cargo is experimentally observed to change the dynamics of key COPII proteins [8], we implement different amounts of cargo and find that the size of the vesicle increases when the cargo load is increased.

Since all membrane bending proteins bend the membrane positively it is not obvious why the COPII vesicle gets a bottle neck shape and why it leaves the membrane. We discuss why this happens within our model.

Contents

1 Introduction **1**

2 Background **3**
2.1 COPII Vesicles - Part of the Secretory Pathway 3
2.2 Membrane Bending Proteins Drive Vesicle Formation 4
2.2.1 Recruitment of the First Main COPII Protein, Sar1 4
2.2.2 Negative Feedback Loop on Sar1 5
2.2.3 Positive Feedback Loop on Sar1 6
2.2.4 Sar1 Induced Curvature 7
2.3 Cargo 8
2.4 The Membrane Bending Model: A Model of Polarized Interacting Particles 10
2.4.1 Particle Interaction 11
2.4.2 Isotropic and Anisotropic Wedging 13
2.4.3 Spherical and Cylindrical Symmetry 15

3 Methods **17**
3.1 Michaelis Menten Kinetics 17
3.2 Numerical Differentiation 18
3.3 Time Scale Separation 19
3.4 Code Structure 20

4 Results **23**
4.1 Regulatory Network of Proteins Driving COPII Formation 23
4.2 The Spatiotemporal Regulatory Network 25
4.3 Spatiotemporal Protein Dynamics on Flat Sheet of Particles 27
4.4 General Parameter Settings When Coupling the Protein Dynamics to the Membrane Bending Model 30
4.5 Vesicle Formation Only Using Isotropic Membrane Bending 31
4.6 Sar1 and Anisotropic Bending 33
4.7 Vesicle Formation Using Isotropic and Anisotropic Membrane Bending . . 35
4.7.1 Vesicle Budding Independent of Protein Dynamics 35
4.7.2 Vesicle Budding Driven by Dynamics of Sar1-Sec Regulatory Network 36
4.7.3 Tube Formation 39
4.8 Budding with PCP Self-organizing in a Circular Pattern 40
4.8.1 Modifying the Particle Interaction to Obtain Self-organizing PCP . 40
4.8.2 Possible Biological Interpretation of β 41
4.8.3 Keeping the Circular Formation in PCP 42
4.8.4 Spontaneously Emerging Circular Pattern in PCP 43
4.8.5 Forming Vesicles from Spontaneously Formed PCP-circles 49
4.9 The Role of Cargo 51

4.9.1 The Amount of Cargo for Vesicle Formation 53
4.9.2 The Size of a Particle 55

5 Discussion and Conclusion **56**
5.1 Question 1 56
5.1.1 Extra Question for Question 1 57
5.2 Question 2 58
5.3 Question 3 60
5.4 Further Research 61

1 Introduction

Proteins for all kinds of different purposes inside or outside of the cell are translated in the Endoplasmic Reticulum (ER). Afterwards they are folded and transported to the destination of their purpose. The majority of the transport from the ER happens at ER exit sites (ERES) through COPII vesicles [25] before they continue along the secretory pathway.

If the transport of proteins within the cell is not working properly, many vital functions stop working. Diseases related to the COPII vesicle formation can happen if one of the essential proteins for COPII vesicle formation is mutated [25]. But diseases like cancer also uses the cell's working secretory pathway to develop. What if the secretory pathway can be known so well that it could be inhibited for infected cells only?

This project focuses on the part of the secretory pathway that is the formation of COPII vesicles. We investigate the interactions between the main actors of the vesicle formation, the COPII proteins, and their roles in the vesicle formation. We do that by writing the regulatory network of their interactions, simplifying it to a simpler model of the *protein dynamics* and coupling this to a model of *membrane bending*. Our two coupled models will be investigated numerically by simulations. But will our simplified models be sufficient to produce vesicles? This leads us to the first question of the project:

How can we couple the model of protein dynamic to the model of membrane bending to replicate COPII vesicle formation?

During the process of answering this question a main subquestion arose. Because this is rather technical this will be presented during the Results chapter 4.

The formation of vesicles in eukaryotic cells happen at many different membranes, and each place has its own set of proteins and mechanisms that cause the budding and scission of the vesicle from the membrane. In many of the budding processes, a so called ESCRT machinery is used to help the separation of the budded vesicle from the membrane by making a contractile ring around the budded vesicle, which pinches it off. The ESCRT machinery seems necessary when the membrane bending actors only do positive membrane curvature. In the COPII vesicle formation the membrane bending proteins only perform positive membrane curvature [13] and no ESCRT machinery is present. Figure 1.1 shows how we expect the COPII vesicle formation to elapse. Until C the size of negative curvature (green) increases. This makes us ask:

How can the COPII vesicle formation get a bottle neck and what causes the scission of the vesicle?

This is going to be discussed in the Discussion chapter 5 when vesicle fission within our model is achieved.

It is often debated how the COPII-dependent secretory pathway can deal with such a variety of cargo proteins . Some types of cargo are for instance larger than the normal sizes of vesicles [25], [28], [2], [6]. In this project we investigate:

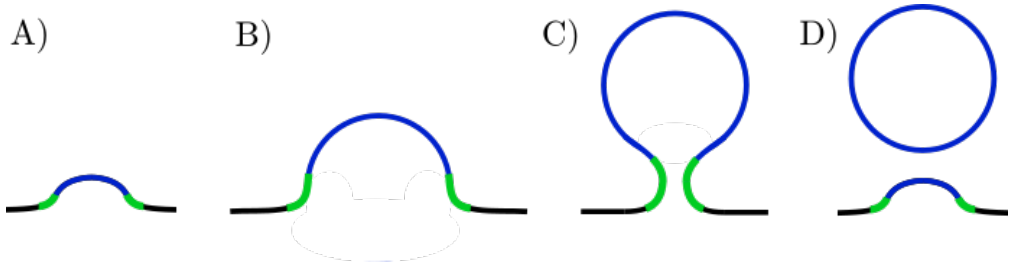

Figure 1.1: A)-D) How we expect the COPII budding process to develop in time. Blue marks positive curvature while green marks negative curvature.

How does cargo influence the vesicle size?

But we only investigate the transport of cargo that can be packed into vesicles of typical vesicle sizes: 60-100 nm [28].

2 Background

In this project we extended a previous built model of polarized interacting particles, which simulated the organization of cells. We modified it to describe interactions between particles of the ER membrane, and I will therefore often refer to the model as the membrane bending model.

In the following sections I present the system of the COPII vesicle formation and after that I present the model of polarized interacting particles.

2.1 COPII Vesicles - Part of the Secretory Pathway

The secretory pathway encompasses the transport of proteins from they are translated and folded at ER, go through the Golgi complex and to their destination that can either be within or outside of the cell. After proper folding, the proteins leave the ER in vesicles called COPII vesicles [25]. The COPII vesicles transport the cargo proteins to the ER-Golgi intermediate compartment (ERGIC) (blue markings in Figure 2.1). From ERGIC, another kind of vesicles, COPI vesicles, transport the cargo proteins to the Golgi complex (red markings in Figure 2.1). From the Golgi complex clathrin-coated vesicles transport the cargo proteins to organelles as the ones mentioned in the figure or to the cell membrane and out of the cell (yellow markings in Figure 2.1).

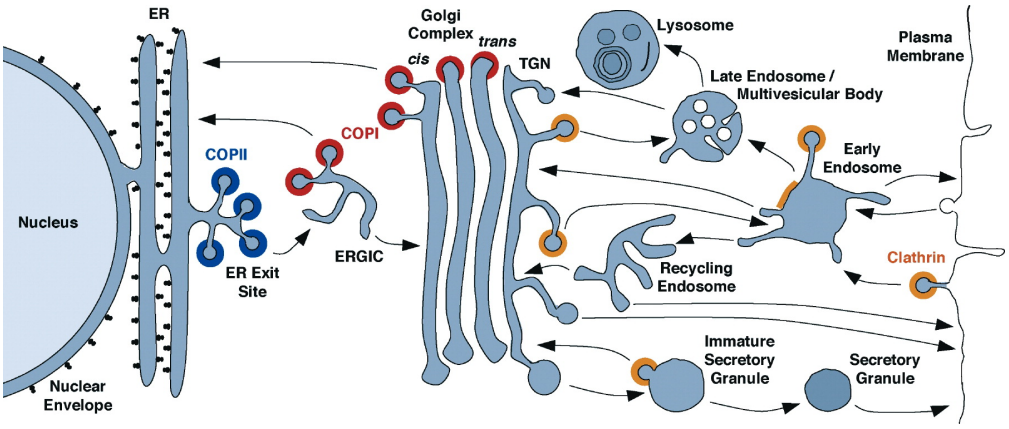

Figure 2.1: The secretory pathway. The dark blue vesicles are COPII, the red vesicles are COPI, and the yellow vesicles are clathrin-coated vesicles. The figure is from [20].

This project is about the formation of COPII vesicles at the ER. The COPII vesicles are formed from a part of the ER's membrane. In the first part of the formation, the ER membrane bends up while recruiting cargo proteins. The half sphere goes into an entire sphere and looses its connection to ER i.e. vesicle fission.

COPII vesicles are typically 60-100 nm in diameter, though COPII vesicles are also able to modify their size to carry larger proteins as procollagen that is 330 nm long [28].

2.2 Membrane Bending Proteins Drive Vesicle Formation

The formation of COPII vesicles is regulated by a chain reaction of proteins recruiting, activating, and deactivating each other. Here I will only derive the central regulating proteins and their interactions.

The formation of the COPII vesicle and the proteins that drive the process, are illustrated in Figure 2.2 taken from [14].

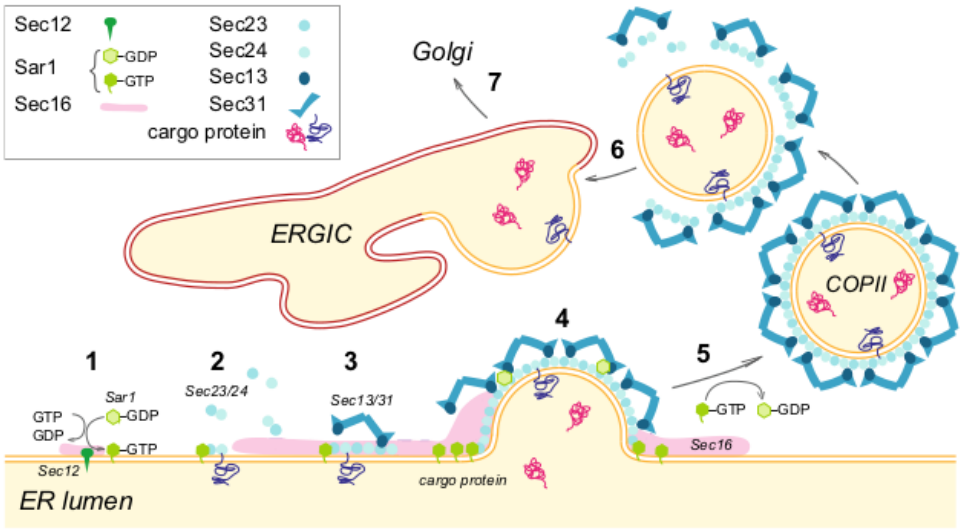

Figure 2.2: COPII vesicle formation and the proteins that drive it. The numbers from 1 to 7 sort the events in chronological order. The figure is taken from [14].

2.2.1 Recruitment of the First Main COPII Protein, Sar1

The central regulator for the vesicle formation is the protein Sar1 (green circles in Figure 2.2). The first thing that happens at 1 in Figure 2.2 is that Sar1 is recruited to the membrane at the ER exit sites (ERESs) by the membrane bound protein: Sec12. Sec12 activates Sar1, meaning that Sar1 goes from its inactive form, Sar1-GDP, to its active form, Sar1-GTP [25]. This is schematically drawn in Figure 2.3a, where the notation $A \rightarrow B$ means that the active protein A upregulates the amount of active B protein by turning some of the inactive B protein into active B protein.

In its active form Sar1's N-terminal helix is exposed and is at the same time inserted into the ER membrane. This creates asymmetry between the inner and outer lipid layer of the ER membrane and leads to membrane curvature [13], [25] (Figure 2.3b from [13]).

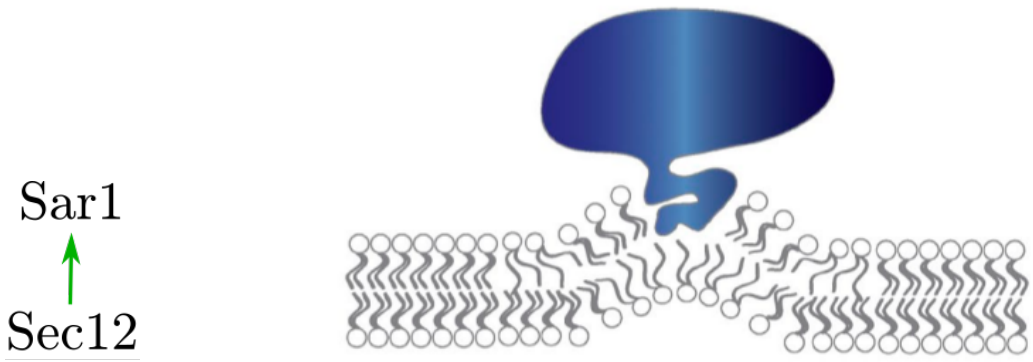

(a) (b)

Figure 2.3: (a) Sec12 activates Sar1 which recruits Sar1 to the ER membrane. (b) The blue shape illustrates Sar1 bending the ER membrane by inserting its N-terminal helix into it. Figure from [13].

2.2.2 Negative Feedback Loop on Sar1

The second thing that happens at 2 in Figure 2.2 is that Sar1 recruits its own inhibitor: the sec23/24 protein complex consisting of the proteins Sec23 and Sec24 [25]. This process, where Sar1 upregulates the concentration of Sec23/24 while Sec23/24 downregulates Sar1, can be identified as a negative feedback loop (Figure 2.4a). Here, the notation $A \dashv B$ means that protein A downregulates the amount of active B protein. That Sar1, as the key actor of the formation, recruits its own inhibitor seems at first glance paradoxical, but as we will see, this process does not stand alone.

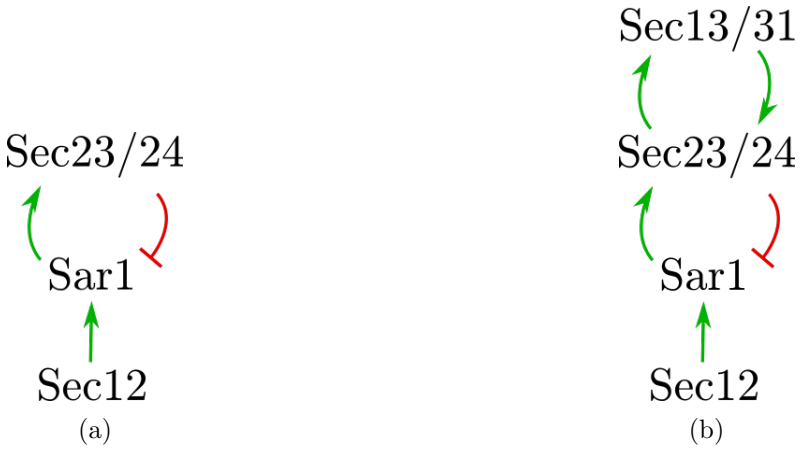

Figure 2.4: (a) Recruitment of Sec23/24 creates a negative feedback loop on Sar1. (b) Including Sec13/31 still makes it a negative feedback loop on Sar1.

The Sec23/24 complex is, together with Sar1, called the inner vesicle coat, but in opposition to Sar1, Sec23/24 stays on the vesicle until the vesicle is formed. A crystal structure of Sar1-Sec23/24 complex is seen in Figure 2.5 taken from [3]. Sec23 deactivates Sar1, while Sec24 has several cargo binding sites and is the one that recruits cargo proteins to the vesicle [6] [21]. Sec23/24 stabilizes or enhances Sar1-generated curvature [7], which is important since Sar1 gets deactivated before the vesicle formation is finished.

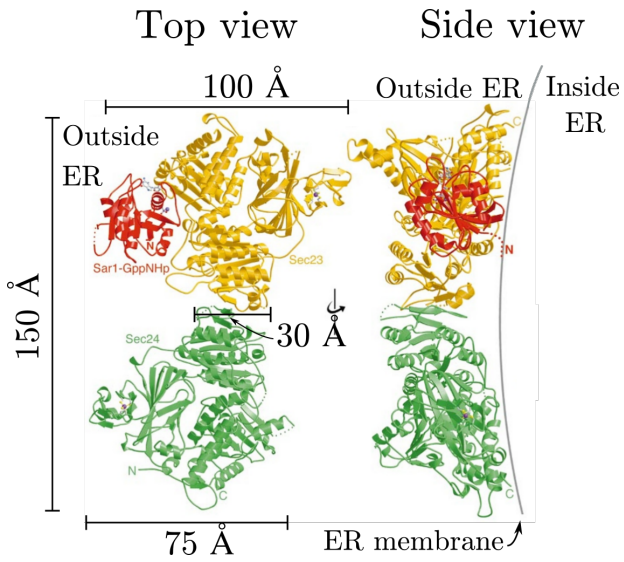

Figure 2.5: Crystal structure of the Sar1-Sec23/24 complex. The red protein is Sar1, the yellow is Sec23 and the green protein is Sec24. The size dimensions as well as the core figure is from [3]

After the Sar1-Sec23/24 complex is recruited to the ER membrane, a larger and rod-shaped protein complex Sec13/31 captures and collects Sar1-Sec23/24 complexes (3 in Figure 2.2). The collection of Sec13/31 forms a lattice structure that turns into polyhedrons[28]. Sec13/31 is also called the outer coat of the vesicle.

Sec31 increases the deactivation done by Sec23 by an order of magnitude [28] [6]. These interactions can be drawn as in Figure 2.4b, where it can be seen that the added feedback loop on Sec23/24 through Sec13/31 is positive, but the overall feedback loop on Sar1 is still negative because number of inhibiting links is uneven.

Sec13/31 is responsible for turning tubes into spherical vesicles [7], possible by arranging the inner coat in smaller patches [29].

2.2.3 Positive Feedback Loop on Sar1

Now the five main COPII coat proteins are mapped into a negative feedback loop, this leaves us with an important unanswered question: After the first Sar1 is recruited to the membrane, what enforces the process of membrane bending to continue in the same area?

From the theory of excitable media we know how to produce a signal that is a pulse that can propagate in space [15]. Such a signal could be the Sar1 concentration, so when a critical amount of Sar1 is bound to the ER-membrane, more will be recruited to that area. Also when a signal in an excitable medium spreads from one point on a 2D plane, it will produce a ring formation [15]. Sar1 is also bound in a ring formation around the borders of the budding vesicle [23]. This suggests that the vesicle formation could be driven from Sar1 acting like an excitable medium. The regulatory network of excitable media consists of one slow negative feedback loop and a fast positive feedback loop [15]. For our signal, the Sar1 concentration, we already have the delayed negative feedback loop but miss the positive feedback loop.

Here Sec16 plays its role. Exactly how Sar1 and Sec16 regulate each other is still being debated [28]. Many suggest that Sec16 works upstream of Sar1 [27], [22] being the one recruiting Sec12 [1]. But Sar1 is also observed to recruit Sec16 to the membrane [27]. Probably Sec16 can both work upstream and downstream of Sar1. This would facilitate a positive feedback loop. This is more directly backed up by [26] where Sec16 and Sar1 is observed to have an interdependent relation where localization of Sec16 to the membrane depends on Sar1-GTP and vice versa.

The positive feedback loop consists of the green arrows going from Sar1 to Sec16 to Sec12 and back again to Sar1 in Figure 2.6. Sec16 also inhibits the deactivation of Sar1 performed by Sec23 and Sec31 [25] this link is drawn as the red line between Sec16 and Sec23/24 in Figure 2.6.

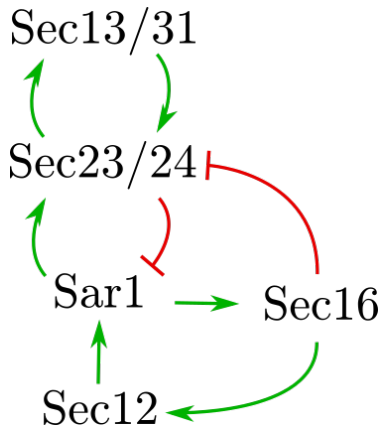

Figure 2.6: The full regulatory network.

With this, the main proteins and their interactions are identified. For simplification these are the ones that will be worked with in this thesis even though many non-mentioned proteins also influence these regulators.

2.2.4 Sar1 Induced Curvature

The observations in this section are essential for our final models of COPII vesicles. Figure 2.7a and 2.7b show results from two experiments performed by [4] and [7] re-

spectively. Both investigates what happens when long time active Sar1 is incubated on spherical liposomes without other COPII proteins. Liposomes consists of a bilipid layer organized in a sphere and in the experiments they function as models of the ER-membrane. Both experiments form membrane structures that are tubular (blue arrows in Figure 2.7). This is in contrast to the spherical COPII vesicles that are seen when the entire COPII machinery is applied. From these observations we are going to hypothesize about how Sar1 bends the ER membrane in section 2.4.3.

The experiments are performed in slightly different ways. In Figure 2.7a they use a mutant of Sar1 that were active and could not be deactivated. In Figure 2.7b they use a wild-type of Sar1 and GTP. Here the concentration of wild-type Sar1 and GTP is probably so high that active Sar1 is always available making the situation similar to the mutant of Sar1. Together these results will be referred to as achieved with a mutant of Sar1.

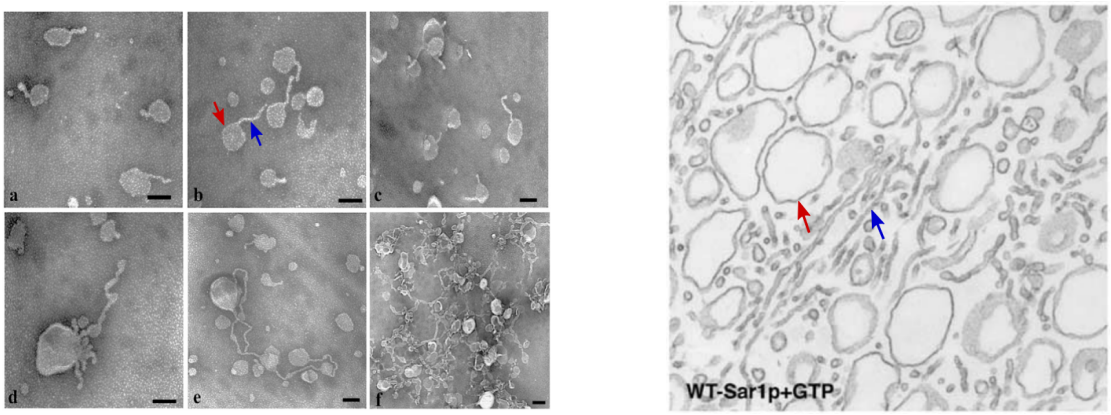

(a) (b)

Figure 2.7: Formation of tubular structures (blue arrows) in two experiments. Both experiments started out with only spherical liposomes (examples of some that are still visible at the red arrows). (a) A mutant of Sar1 is used, that can not be deactivated. Figure from [4]. (b) The Sar1 used is a wild-type Sar1 in the presence of GTP that activates it. Figure from [7].

2.3 Cargo

Now the dynamics of the main COPII proteins are covered, but what about the cargo proteins, which the vesicle is made to transport? Are they passive passengers or do they influence the vesicle?

Cargo can play a role in several ways [25], some are mentioned here. Cargo changes the turnover rate of the COPII proteins [25], [8]. The turnover rate is the rate at which new particles bind to the ER membrane. Fortser et al. [8] have done experiments with Flourescence Recovery After Photobleaching (FRAP) in living cells at a single ERES

(Figure 2.8). Here COPII proteins are YFP-tagged[1] and emit fluorescent light. They bleach a single ERES, which means that the fluorescent signal decreases. But because of the turnover of particles from bleached to non-bleached particles the signal increases again. The turnover is then measured as the time it takes to recover halfway to the original signal which is called the half time. This recovery to the signal before photo bleaching is plotted in Figure 2.8.

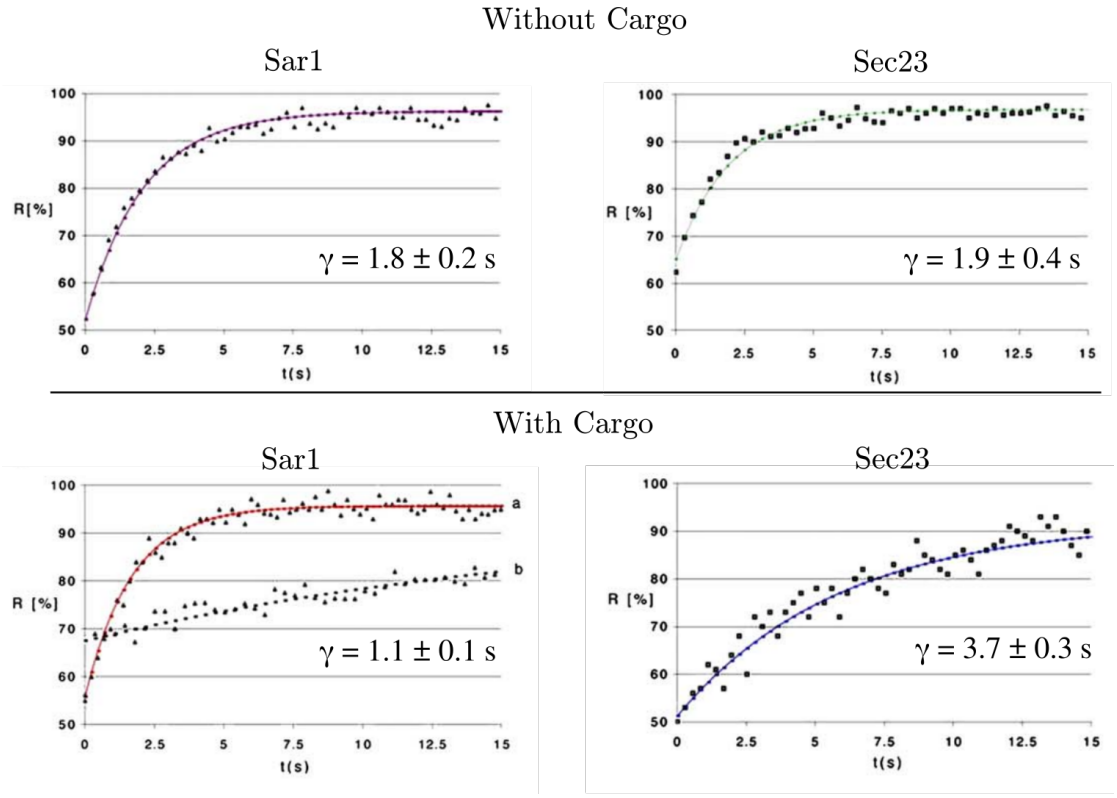

Figure 2.8: Recovery after photobleaching obtained by [8]. γ is the time it takes for the system to reach halfway between the fluorescence level at t=0 and the level at steady state. This half time is cargo dependent.

Figure 2.8 shows the half time of recovery, γ, for Sar1 and Sec23 without and with cargo. Without cargo the half time for Sar1 and Sec23 1.8 ± 0.2 s and 1.9 ± 0.4 s respectively, meaning that they are equally large, both around 2 s. In general Sar1 leaves the budding vesicle before the vesicle formation is finished, but when the turnover rate for Sec23 is the same as for Sar1, does Sec23 then also leave the budding vesicle before it is finished? This would prevent vesicle formation. This worry is eliminated when cargo is present. With cargo, the half time of Sec23 is four times higher than that of Sar1: 3.7 ± 0.3 for Sec23 and 1.1 ± 0.1 for Sar1. This makes it possible that Sar1 leaves the vesicle formation before it is finished while Sec23 stays on.

[1]YFP: Yellow Flourescent Protein

Another way cargo can influence the vesicle formation is through Sec24 to change the angle between hinges between the Sec13/31 rods. This makes it possible for the outer coat of the vesicle to adopt various sizes and geometries [25]. This inspires us to investigate whether our model with cargo implemented can produce vesicles of different sizes dependent on the amount of cargo present (section 4.9). It is an entire field of investigation how vesicles can carry proteins larger than the normal size of vesicles 60-100 nm, we will keep our investigations regarding cargo to the secretion of cargo in the typical range of vesicle sizes 60-100 nm.

2.4 The Membrane Bending Model: A Model of Polarized Interacting Particles

To model the ER membrane and membrane bending processes, we have used a model of polarized interacting particles. This model has earlier been used to model cell to cell interaction in the process of forming organ structures [5], [9], [24]. In this project, a particle is defined as a point particle, where the equilibrium distance between their centers is 23.5 nm (Figure 2.9, calculated in section 4.9.2). The equilibrium distance corresponds to the size of a particle. The simulation models a square of the ER membrane of 700 nm in width, which corresponds to the size of a large ERES.

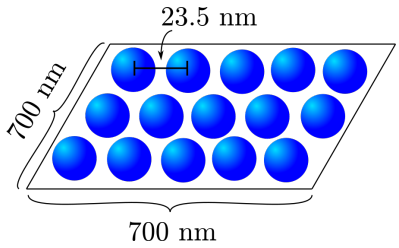

Figure 2.9: Sketch of a flat sheet of particles. The sizes are found in section 4.9.2

To apply the model to the ER membrane, we need to justify that a particle of the ER membrane is polarized. The ER membrane consists of lipid bilayers. One lipid pair orient themselves along a geometric axis pointing in and out of the membrane, because their hydrophilic headgroups want to be either on the inside or outside of the membrane, while the hydrophobic tails are inside the membrane. Cells also orient themselves along a geometric axis and this ability is called cell polarity. In the same way it can be said that a pair of lipids in the blue ring is polarized along the blue double arrow in Figure 2.10 A, core of figure is taken from [19].

But in contradiction to cells, a pair of lipids can be similar on the inside and outside of the ER membrane. But this symmetry is broken when a particle in our model is defined as being a small part of the ER membrane. Actually our ER membrane particle has a diameter of 23.5 nm while a lipid headgroup has a diameter of 0.5 nm [16], so one particle would represent approximately 2000 lipid pairs.But the ER membrane also consists of membrane bound proteins, which break the in-out symmetry (Figure 2.10 B).

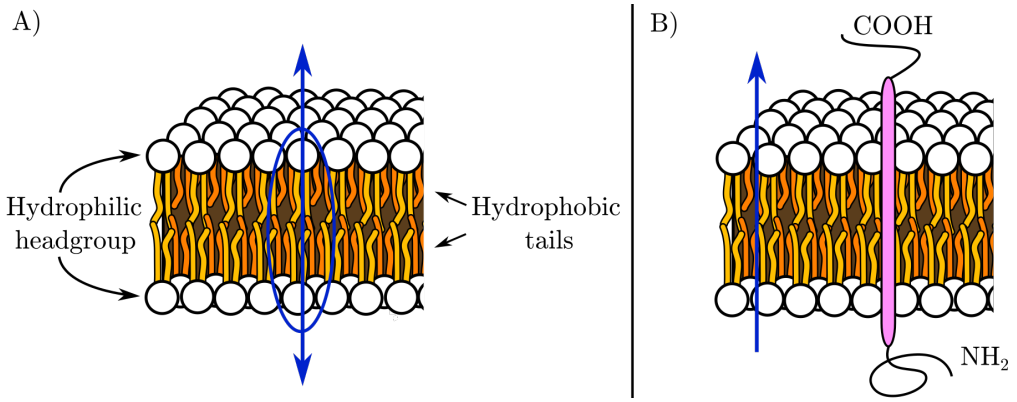

Figure 2.10: A) Lipid pairs in bilayers orient themselves according to the blue arrow. B) The pink transmembrane protein makes the entire ER membrane have a defined inside and outside. The illustration of the lipid bilayer is from [19].

The polarization, that defines what is the inside and outside of the membrane, is called apical-basal (AB) polarity (simplified illustration in Figure 2.11a. The symmetry of a particle could also be broken in the direction along the membrane sheet, this would lead to another polarization of the particle which is called Planar Cell Polarity (PCP) using the jargon from cell polarity (Figure 2.11b). Each particle in the me model is assigned with a positional vector and the two polarity vectors (Figure 2.11).

(a) (b)

Figure 2.11: The two particle polarities point in the direction of symmetry breaking. (a) The apical-basal (AB) polarity points out of the membrane. (b) The planar cell polarity (PCP) points along the membrane.

2.4.1 Particle Interaction

The particles interact pairwise as point particles through the inter-particle potential

$$V_{ij} = e^{-\bar{r}_{ij}} - S\ e^{-\bar{r}_{ij}/c}. \tag{2.1}$$

Here $\bar{\mathbf{r}}_{ij}$ is the vector between the placement of the pair of particles. c is set to 5 through the entire project and ensures that the equilibrium distance between particles

corresponds to 2 of the model's spatial units. This can be found in the case where $S = 1$ by isolating r in $\frac{dV}{d\bar{r}} = 0$. The first term in the potential corresponds to repulsion and the second term to attraction, as long as S is positive. S sets the strength of the attraction term and is defined as

$$S = \lambda_1 S_1 + \lambda_2 S_2 \tag{2.2}$$

Here S_1 and S_2 are defined in Eq. (2.3) and determines how the AB-polarity vector noted $\hat{p}$ and the PCP-vector noted $\hat{q}$ should be orientated in relation to the directional unit vector, $\hat{r}$, to achieve the strongest attraction, $S_1 = S_2 = 1$, or the strongest repulsion $S_1 = S_2 = -1$. The λs are numbers between 0 and 1 and should sum to 1 to retain a constant equilibrium distance [5]. The λ-values determine which polarity interactions are most heavily weighted.

$$S_1 = (\hat{p}_i \times \hat{r}_{ij}) \cdot (\hat{p}_j \times \hat{r}_{ij}), \qquad S_2 = (\hat{p}_i \times \hat{q}_i) \cdot (\hat{p}_j \times \hat{q}_j) \tag{2.3}$$

When $\lambda_1 = 1$ and $\lambda_2 = 0$, the favourable minimal energy state of the system is when both $\hat{p}_i$ and $\hat{p}_j$ are perpendicular to $\hat{r}_{ij}$, and when the interacting particles have parallel $\hat{p}$ (Figure 2.12 B). This would make S positive and the potential will favour a certain distance between the particles. Antiparallel $\hat{p}$s would make S negative and also make the overall potential positive and repulsive (Figure 2.12 A, taken from [5]). When $\lambda_1 = 1$ and $\lambda_2 = 0$, $\hat{q}$ is no longer of importance and could as well never have been there. When $\lambda_2 \neq 0$ the energy cost of the system is minimized when pairwise $\hat{q}$s are parallel to each other but perpendicular to their $\hat{p}$s (Figure 2.12 C).

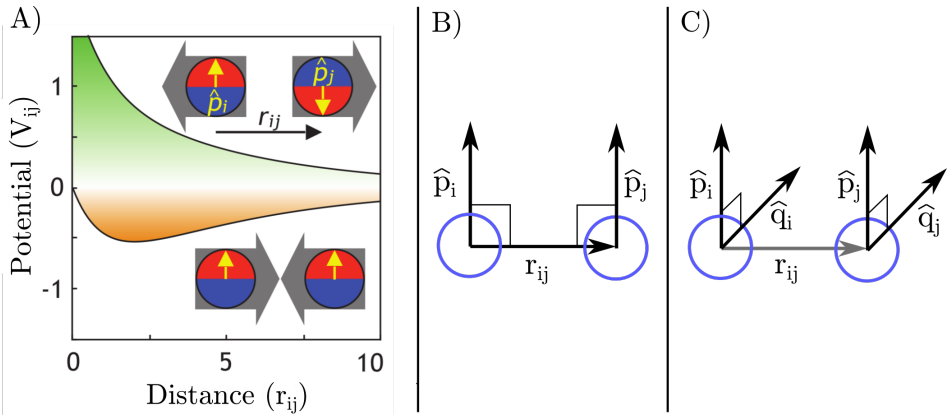

Figure 2.12: A) If neighbouring particles have antiparallel $\hat{p}$-vectors, they will repulse each other, because the potential only can be minimized if the distance between them becomes bigger. If $\hat{p}$-vectors are parallel, they have a favoured equilibrium distance which will hold them together. Figure is taken from [5]. B) The orientation of $\hat{p}$ that minimizes the potential energy ($\lambda_1 = 1$ and $\lambda_2 = 0$). C) The orientation of $\hat{p}$ and $\hat{q}$ that minimizes the potential energy ($\lambda_1 = \lambda_2 = 0.5$).

The pairwise interaction is only between neighbouring particles, which is defined from a Voronoi diagram. Here, lines are drawn such that all points along the line have equal distance to the nearest particles, only particles that share such a line without intersections are Voronoi neighbours (Figure 2.13, taken from [5]).

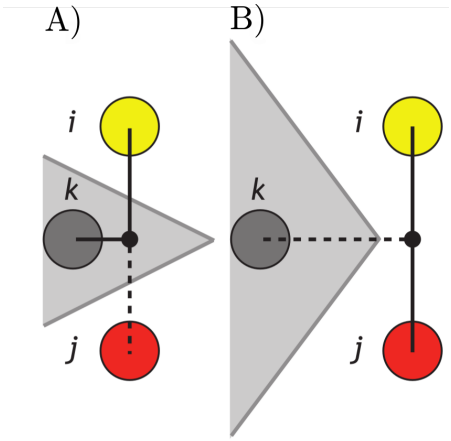

Figure 2.13: Voronoi diagram. A) The yellow and red particles are not Voronoi neighbours because the direct line between them is intersected by the Voronoi diagram for the gray particle. B) The yellow and red particles are Voronoi neighbours. Figure is taken from [5]

The total potential of a particle, i, is the sum of its interactions with its neighbours, j, as

$$V_i = \sum_j V_{ij}. \tag{2.4}$$

The motion of a particle is assumed to have overdamped Langevin dynamics and the change in position as well at the direction of the vectors $\hat{p}$ and $\hat{q}$, are found as in Eq. (2.5), where η is random uncorrelated Gaussian noise.

$$\frac{d\hat{r}_i}{dt} = -\frac{dV_i}{d\hat{r}_i} + \eta, \qquad \frac{d\hat{p}_i}{dt} = -\frac{dV_i}{d\hat{p}_i} + \eta, \qquad \text{and} \qquad \frac{d\hat{q}_i}{dt} = -\frac{dV_i}{d\hat{q}_i} + \eta. \tag{2.5}$$

2.4.2 Isotropic and Anisotropic Wedging

S in Eq. (2.3) favours parallel AB-vectors, $\hat{p}$, and parallel PCP-vectors, $\hat{q}$. Simulations are most often started with a flat sheet of particles while $\hat{p}$ points out of the sheet plane and $\hat{q}$ points parallel along the plane. But using S in Eq. (2.3) on this starting condition would make no changes to $\hat{r}$, $\hat{p}$, nor $\hat{q}$, and the sheet of particles would stay flat. The shape of a particle that would not bend the sheet is a non-wedged particle (top of Figure 2.14 A). The amount of wedging is described by the angle, α, which will be defined below.

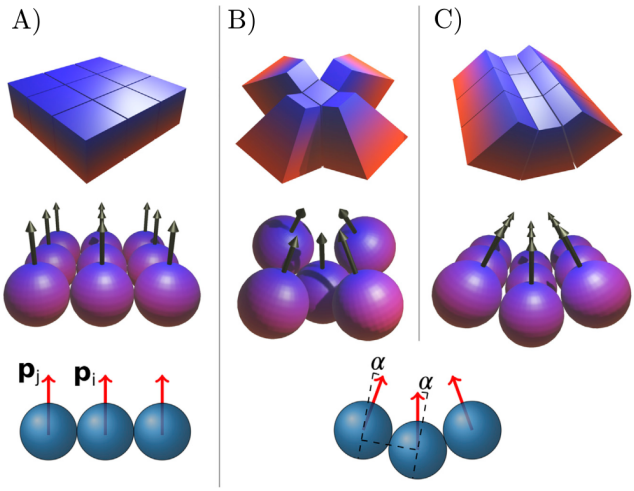

Figure 2.14: A) No wedging ($\alpha = 0$). B) Isotropic wedging. The favoured angle is the same in all directions. C) Anisotropic wedging. The angle α is preferred in a particular direction. Figure is from [9].

For the sheet to bend, angles between the AB-polarity vectors must be energetic favored. If the same angle is favoured in all directions along the sheet, the particles have *isotropic* wedging (Figure 2.14 B). Implementation of a favoured angle, α, can be interpreted as the particles becoming wedge shaped, and together they will prefer organizing in spherical structures.

If the angle is favoured in a particular direction, seen from the perspective of a particle, the particle is said to have *anisotropic* wedging (Figure 2.14 C). This could be interpreted as the shape of the particle that is wedged in one direction but not in the perpendicular direction. Particles with such a shape would prefer to organize in a cylindrical structure.

To implement the isotropic or anisotropic angle between AB-vectors, $\hat{p}$ is redefined. $\hat{p}_i$ becomes $\tilde{p}_i$ according to Eq. (2.6). Here, the denominator is for the sake of normalization, which also makes $\tilde{p}$ a unit vector. α is the length of the side in the right-angled triangle opposite the angle between $\hat{p}$ and $\tilde{p}$, see Figure 2.15. α corresponds to the angle between $\hat{p}$ and $\tilde{p}$. When α is small the length α is very precisely the angle, α', in radians. In the model, each particle is assigned an α and the α seen in Eq. (2.6) is an average of the αs of the two neighboring particles. $\langle\hat{q}\rangle_{ij}$ is the average of the two interacting particles' $\hat{q}$s.

$$\begin{aligned} \tilde{p}_i &= \frac{\hat{p}_i - \alpha\hat{r}_{ij}}{|\hat{p}_i - \alpha\hat{r}_{ij}|} \qquad \text{(isotropic wedging)} \\ \tilde{p}_i &= \frac{\hat{p}_i - \alpha\langle\hat{q}\rangle_{ij}}{|\hat{p}_i - \alpha\langle\hat{q}\rangle_{ij}|} \qquad \text{(anisotropic wedging)} \end{aligned} \tag{2.6}$$

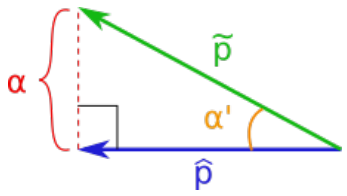

Figure 2.15: Definition of α. In this illustration $\tilde{p}$ is not yet normalized. α is a length, but for small α $\alpha = \alpha'$.

The $\hat{p}$-vector of the neighbour is also corrected during the interaction when α is applied. It is corrected nearly the same way but with positive signs Eq. (2.7)). This means that the entire angle between $\tilde{p}_i$ and $\tilde{p}_j$ is two times α'.

$$\begin{aligned} \tilde{p}_i &= \frac{\hat{p}_j + \alpha \hat{r}_{ij}}{|\hat{p}_j + \alpha \hat{r}_{ij}|} \qquad \text{(isotropic wedging)} \\ \tilde{p}_i &= \frac{\hat{p}_j + \alpha \langle \hat{q} \rangle_{ij}}{|\hat{p}_j + \alpha \langle \hat{q} \rangle_{ij}|} \qquad \text{(anisotropic wedging)} \end{aligned} \tag{2.7}$$

2.4.3 Spherical and Cylindrical Symmetry

Experimental observations show that the COPII machinery is able to produce both spherical vesicles as well as tubes [4], [7]. How can these structures be obtained within the model of polarized interacting particles?

The spherical structures can be obtained by favouring an isotropic bend between the AB-polarity vectors $\hat{p}$ while there is no need for having PCP in the system and λs can as well be set to: $\lambda_1 = 1$ and $\lambda_2 = 0$.

To obtain cylindrical structures PCP is needed and the angle between AB-polarity vectors should be anisotropic. But this is not enough. Anisotropic bending makes the particles favour bending along certain directions, determined by PCP which can vary from particle to particle. But to form a tube there must be a global direction with no bending along the tube axis. So how to achieve a global direction with no bending, when anisotropy is determined locally?

Previous work [9] showed that this can be achieved by anisotropic bending and tangential circular orientation of the PCP (Figure 2.16a). But to explain it a little more, here come some lines of thought.

Firstly it can be seen from the anisotropic corrected $\tilde{p}$ Eq. (2.6), that the direction with the most bending is along $\langle \hat{q} \rangle_{ij}$. Also if $\hat{p}_i$ and $\langle \hat{q} \rangle_{ij}$ are not entirely perpendicular, and $\tilde{p}_i$ is corrected along $\hat{p}$, it will just be cancelled by the normalization. This means that the direction with no bend is perpendicular to both $\hat{p}_i$ and $\langle \hat{q} \rangle_{ij}$, and it is this direction that we want to be the same for all particles to make a cylinder. Lets see what happens when PCP initially is put in a circular pattern as showed in Figure 2.16a. Here a flat sheet is seen from the top, the black arrows show PCP, which is also the direction

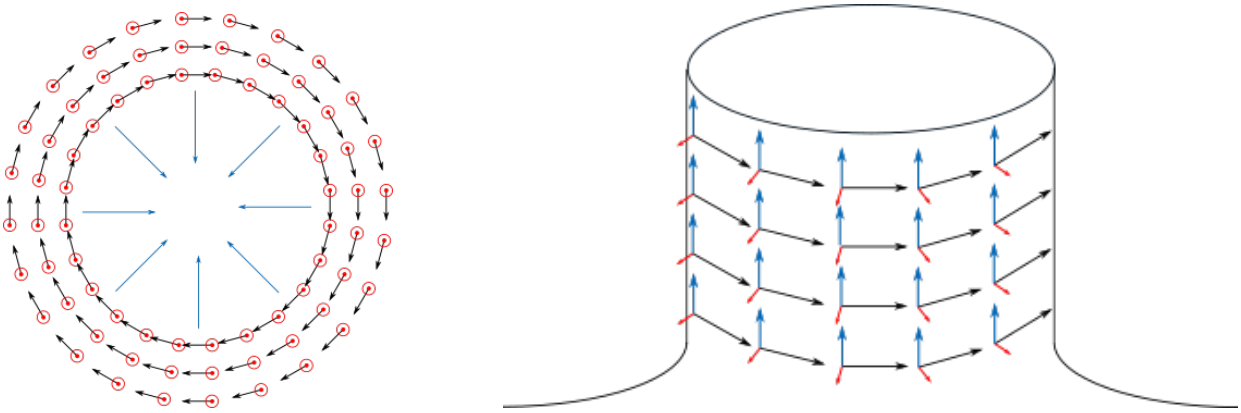

(a) (b)

Figure 2.16: Forming a cylinder. Black vectors are PCP. Red vectors are AB polarity. Blue arrows points in a direction perpendicular to PCP and AB-polarity, where the system prefers no bending. (a) Initial condition: A flat sheet is seen from the top. (b) A lower energy state of the system is found when the sheet forms a cylinder.

The symmetry ...	**... is obtained by having the settings:**
Spherical	Isotropic membrane bend. No PCP: $\lambda_1 = 1$, $\lambda_2 = 0$.
Cylindrical	Anisotropic membrane bend. PCP in circular pattern, $\lambda_1 = \lambda_2 = 0.5$.

Table 2.1: The needed settings to obtain the two symmetries: spherical and cylindrical.

that the sheet would like to bend in, the red points mark AB polarity going out of the plane, and the blue arrows point radially inwards to mark the direction with no bend. In this situation, the sheet is not bend in the direction that it would like to; along PCP. To minimize the energy, the sheet can push the particles up in the middle, creating a cylinder as seen on Figure 2.16b. On the cylinder, the particles have arranged to satisfy that the sheet bends along PCP but not along the blue arrows. The settings to achieve the two symmetries are summed up in Table 2.1.

To create the circular pattern of PCP, it can be fixed to follow Eq. (2.8) to obtain the cylindrical symmetry. Here $\hat{z}$ is the unit vector in the z-direction perpendicular to the plane of particles, and $\hat{r}_{xy}$ is a vector that describes the placement of the particle within the sheet plane. The origin of the coordinate system is placed in the middle of the sheet of particles.

$$\hat{q} = \hat{z} \times \hat{r}_{xy} \tag{2.8}$$

3 Methods

In this project we couple two models: *the membrane bending model* (section 2.4) and the the model of *protein dynamics* (section 2.2). They are coupled the such that the model of protein dynamics are going to drive the membrane bending model. The coupling is going to happen through the first order differential equations of the models. For the membrane bending model differential equations are already found in Eq. (2.5), though they will later be modified a bit. For the model of protein dynamics the interactions have been mapped into a regulatory network, but the differential equations will be written up in the Results section. To transform the regulatory network of COPII proteins into differential equations we use a model of enzyme-kinetics, *Michaelis Menten kinetics*, described in next section. How these differential equations are used to update key variables is described in section 3.2. In section 3.3 I will describe how we handled issues about different time scales of the two models when coupling them. In last section of this chapter I will show an overview of the flow of the main part of the code.

3.1 Michaelis Menten Kinetics

We will use the model of Michealis Menten kinetics to translate a regulatory network of proteins, such as Figure 2.6, into a set of differential equations.

Michaelis Menten kinetics describes how enzymes affect the production rate of the product they catalyze. Enzymes increase the reaction rate for a substrate going into a product without being consumed themselves. More specifically they do it as seen in the reaction scheme 3.1. Here the enzyme, E, goes into a complex with the substrate, S, with the rate k_1. This substrate can either fall apart into substrate and enzyme again with the rate k_2, or the substrate is turned into the product, P, and enzyme with the rate k_3.

$$E + S \underset{k_1}{\overset{k_2}{\rightleftharpoons}} [ES] \overset{k_3}{\rightarrow} E + P. \tag{3.1}$$

This is similar to the processes seen earlier where activated protein A upregulates the amount of active B proteins, $A \rightarrow B$. Here A is the enzyme and B is the product, while the substrate is the inactive B protein. To use the E, S, and P notation this would correspond to $E \rightarrow P$.

Looking at the reaction scheme 3.1 we see that the change in P is proportional to rate k_3 and to the amount of [ES] complexes. Therefore we can write

$$\frac{dP}{dt} = k_3[ES]. \tag{3.2}$$

To specify the rate of the product further, it is assumed that the enzyme-substrate complex, [ES], is in steady state:

$$\frac{d[ES]}{dt} = k_1 - k_2 \cdot [ES] - k_3 \cdot [ES] = 0 \Rightarrow [ES] = \frac{k_1 \cdot E \cdot S}{k_2 + k_3} = \frac{E \cdot S}{k_M} \tag{3.3}$$

Here the constants are collected into the Michaelis Menten constant $k_M = \frac{k_2+k_3}{k_1}$. Furthermore the total amount of enzyme, E^T, is introduced as: $E^T = E+[ES]$. Isolating E, and inserting this into Eq. (3.3) gives:

$$[ES] = (E^T - [ES])\frac{S}{k_M} \Leftrightarrow [ES] = \frac{E^T \cdot S}{k_M + S}. \tag{3.4}$$

Inserting this expression for [ES] back into the expression for the production rate gives:

$$\frac{dP}{dt} = k_3 E^T \frac{S}{S + k_M}. \tag{3.5}$$

As said the substrate corresponds to the inactive B proteins. The total amount of B protein, B^T, is assumed constant in time. $B^T = B + B^i$, where the superscript i notes the inactive B protein, and B without superscript is the the active B protein. Therefore the substrate can also be written: $B^i = B^T - B$. Inferring this in Eq. (3.5), the rate for the production of active B protein, B, is:

$$\frac{dB}{dt} = k \cdot A^T \frac{B^T - B}{B^T - B + k_M}. \tag{3.6}$$

If protein A on the other hand deactivates protein B, the schematic notation is as in Eq. (3.7). The change in the amount of active B proteins is then written as in Eq. (3.8), where the substrate is now the amount of active B.

$$A \dashv B \tag{3.7}$$

$$\frac{dB}{dt} = -k \cdot A^T \frac{B}{B + k_M}. \tag{3.8}$$

With this we should be able to translate the regulatory network of the COPII proteins into a set of differential equations.

3.2 Numerical Differentiation

The variables of the model are updated from knowledge of their temporal, first order differential equations $\frac{dy}{dt}$. These changes are then applied in a combination of the Euler method and by calculating their algebraic gradient.

In the Euler method the variables, as well as time, are discretized. The array of a discretized variable, y, is found step by step, by iterating the expression seen in Eq. (3.9). Here, k represents a certain time step, Δt is the size of the time step, and Δy_k is sometimes calculated as the difference between y_k and y_{k-1}, but in our models we use the theoretical gradient $\frac{dy_k}{dt}$.

$$y_{k+1} = y_k + \Delta t \cdot \Delta y_k = y_k + \Delta t \cdot \frac{dy_k}{dt} \tag{3.9}$$

For the protein concentrations expressions for their gradients will be found with the method of Michaelis Menten kinetics.

For the position and polarity vectors, the gradients are differential expressions of the potential, V_i, Eq. (2.5). It is very demanding to find the algebraic expressions of these gradients. Instead of finding the algebraic expression first where after they are evaluated for specific values of $\hat{r}$, $\hat{p}$, and $\hat{q}$, the process of evaluating is happening alongside of the differentiation. The method is called *automatic differentiation* and is as precise as the symbolic differentiation, but it demands much less computer power. This make sense since we also end out with less information about the gradient; instead of an algebraic expression we just get a value for that specific gradient. When doing automatic differentiation, the function $V_i(\hat{r}, \hat{p}, \hat{q})$ is decomposed into its mathematical operations. To take a more simple example, lets work with $y(x) = 3 \cdot e^{sin(x)}$ instead. This can be decomposed into $y = f(g(h(x)))$, where

$$y = f(x_2) = 3 \cdot x_2, \quad x_2 = g(x_1) = e^{x_1}, \text{ and } \quad x_1 = h(x) = sin(x). \tag{3.10}$$

Hereafter the chain rule can be applied:

$$\frac{dy}{dx} = \frac{dy}{dx_2}\frac{dx_2}{dx_1}\frac{dx_1}{dx} = \frac{df(x_2)}{dx_2}\frac{dg(x_1)}{dx_1}\frac{dh(x)}{dx}. \tag{3.11}$$

The procedure is then to differentiate each differential expression separately and evaluate them in the specific point, e.g. $x = 0$ [18]. To evaluate each differential expression, the values for x_1 and x_2 are needed but can easily be found by inserting $x = 0$ into $x_1 = h(x = 0) = sin(0) = 0$ and $x_2 = g(x_1) = e^{x_1} = e^0 = 1$. This gives the evaluated differential values:

$$\left.\frac{df(x_2)}{dx_2}\right|_{x=0} = 3 \cdot x_2 = 3 \cdot 1 = 3, \quad \left.\frac{dg(x_1)}{dx_1}\right|_{x=0} = e^{x_1} = e^0 = 1, \quad \left.\frac{dh(x)}{dx}\right|_{x=0} = cos(0) = 1. \tag{3.12}$$

When the derivatives are evaluated, their values can be multiplied according to the chain rule and a numerical value for entire gradient can be found. Our example gives

$$\left.\frac{dy}{dx}\right|_{x=1} = 3 \cdot 1 \cdot 1 = 3. \tag{3.13}$$

To do the automatic differentiation in this model, a package from the PyTorch library is used: `torch.autograd`.

3.3 Time Scale Separation

When coupling our two models, the proteins dynamics are going to drive the membrane bending, so when the protein concentrations are updated, new settings for the membrane bending model are applied. But the membrane bending model needs time to reach the steady state given these settings. This is solved by updating the membrane bending

model a given number of times (blue lines in Figure 3.1) before updating the model of protein dynamics (red lines in Figure 3.1).

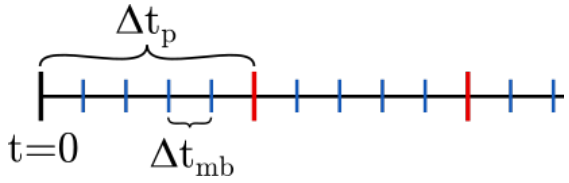

Figure 3.1: Time scale separation. Δt_p is the time step for updating the protein kinetics and has the units of seconds. The $\Delta t_m b$ is the intermediary time step for the membrane bending model and has the units of $\frac{1}{N}$ s, where N is the number of blue time steps between each red time step.

In our simulations, the Δt_p for the protein dynamics has the same numerical value as $\Delta t_m b$ for the membrane bending model, which means that the timescale of the protein dynamics cannot have the same units as the timescale for the membrane bending.

Since the half life of the membrane bound proteins are known in seconds, the Δt_p also has the units of seconds. This means that the unit of the intermediary steps $\Delta t_m b$ is $\frac{1}{N}$ s, where N is the number of intermediary time steps between each update of the protein concentrations. N should be big enough for the membrane bending to reach steady state. This value has not been investigated in detail, but since we later show simulations where the membrane is bending according to the protein concentration, we are at least in the limit where the bending of the membrane can catch somewhat up with the changes in protein dynamics. Simulations until section 4.8.4 have $N = 500$ and from then on simulations have $N = 1500$. To find the time in seconds for membrane bending simulations that is independent of protein dynamics, their time scale is multiplied with a factor of $\frac{1}{N}$ where N has the same order of magnitude as 500 and 1500, namely: $\frac{1}{1000}$ s.

3.4 Code Structure

Here I am going to show the structure of the code when the membrane bending is coupled to the protein dynamics. I am not going to include the initializing functions. The code loop over the processes in Figure 3.2.

The entire code can be found on [1].

Updating nearest neighbours

Out of the 910 particles, a list of the 30-200 nearest neighbours is in the beginning updated each time step, but later only every 20th time step. The neighbours are found by using the function `scipy.spatial.cKDTree()` from the scipy package, which is called within the function `find_potential_neighbours()` defined in the code. Since it is not

[1] `https://github.com/halloumamad/COPII_vesicle_formation`

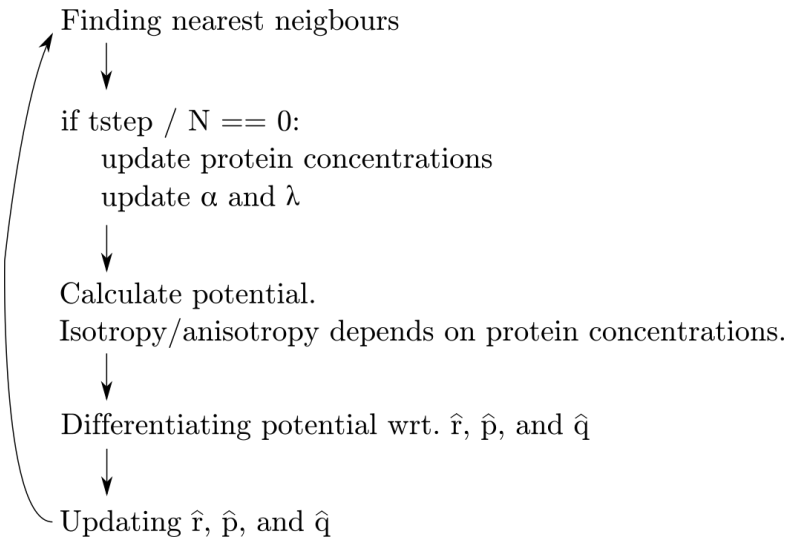

Figure 3.2: Structure of the code excluding the initializing functions. N is the number of intermediate time steps creating the timescale separation.

necessarily called in each iteration, the list can be slightly wrong and is therefore called "potential neighbours".

From this list the true neighbours are found in each iteration using the function code defined `find_true_neighbours()`. Here, the nearest neighbours are found by calculating the distance between each set of potential neighbours with Pythagoras.

Updating protein concentrations and coupling the two systems

The first time step and each N time step the Sar1 and Sec concentrations are updated according to the Euler method. N is the number of intermediary time steps and perform the time scale separation. The $\frac{dA}{dt}$ and $\frac{dE}{dt}$ used in the Euler method are functions we define in the code with the names `dA_dt()` and `dE_dt()`. How they are going to be defined is written in the results section 4.2.

The membrane bending model is coupled to the protein kinetics by relating the parameters α and λ to the protein concentrations. Exactly how this is done will be presented during the results.

Calculating the potential

In the function `potential()` all pairwise potentials between nearest neighbours are calculated and summed together. When coupling the membrane bending to the protein concentration the pairwise potential is calculated using isotropic bending or anisotropic bending based on the level of protein concentrations in each particle.

Differentiating the potential

Differentiating the potential is done with the PyTorch package `torch.autograd`.

Updating $\hat{r}$, $\hat{p}$, and $\hat{q}$

With the differential expression just found, $\hat{r}$, $\hat{p}$, and $\hat{q}$ are updated according to Eq. (2.5) using the Euler method.

4 Results

In this chapter we will first simplify the regulatory network, and from this write up the model for the dynamics of the COPII proteins. Then we will couple this model of *protein dynamics* to the *membrane bending* model, where we will try out different ways Sar1 could bend the ER membrane and we suggest how this could be biologically meaningful. This is all in investigation of the first question asked in the introduction:

How can we couple the model of protein dynamic to the model of membrane bending to replicate COPII vesicle formation?

During this process we had to investigate how we could modify original membrane bending model to make the PCP vector self organize the way we needed it to organize. This investigation and how our modification could be biologically interpreted is found in section 4.8. Lastly we investigate how cargo influences the size of the vesicles (section 4.9).

4.1 Regulatory Network of Proteins Driving COPII Formation

In section 2.2 we drew the regulatory network that we would like to model (reprinted in Figure 4.1a). But before we write up the differential equations for the changes in protein concentration we want to simplify this network. As mentioned in section 2.2.3, Sar1 acting like an excitable medium could drive the vesicle formation, and for Sar1 to be an excitable medium, only a slow negative feedback loop and fast positive feedback loop on Sar1 is needed. This leads to the simplification seen in Figure 4.1b.

One simplification is that Sec23/24 and Sec13/31 have been grouped into one actor, Sec. When grouping these Sec proteins the strength of the inhibition of Sar1 can be modified to represent the effective inhibition from the four Sec proteins together.

Another simplification is simplifying the positive feedback loop from Sar1 through Sec16 and Sec12 and back to Sar1 again. We represent this by a positive feedback loop from and to Sar1. The inhibition from Sec16 on the Sec proteins could still be present by a modification to the inhibition from Sec on Sar1.

A support for the positive feedback loop that is beyond Sec16, is that it is also observed that the binding affinity of attaching Sar1 to the ER membrane is higher for membranes with higher curvature [10]. So when Sar1 attaches to the membrane it bends the membrane, and this bend induces even more Sar1 to bind in the area, hence creating a positive feedback.

All proteins in a regulatory network has a basal removal rate, which is the half life of the protein on the membrane in the absence of any other actor from the network influencing it. Because it is generic it is often left out of illustrations of the networks. In Figure 4.1c basal removal is included as the inhibition lines on Sec and Sar1 from the left. The constants along each link in Figure 4.1c is the rate of the interaction.

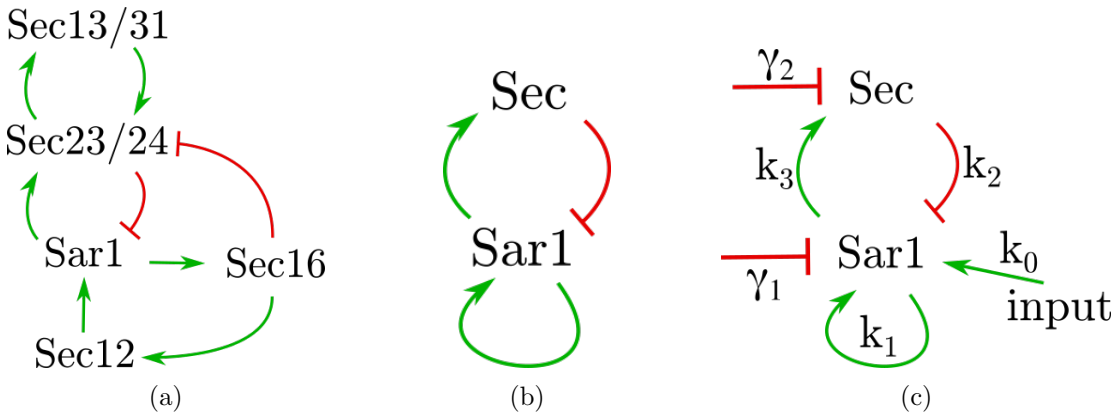

Figure 4.1: (a) The full regulatory network. (b) The simplified regulatory network. (c) The simplified regulatory network with basal removal shown as inhibition lines from the left on each protein as well as the input of the system. The rates are written along each interaction line.

To excite the system, meaning for Sar1 to start increasing, an external input is need. This is also drawn in Figure 4.1c.

By using the Michaelis Menten kinetics explained in section 3.1, the changes in protein concentrations can be written up from the network in Figure 4.1c. This gives two coupled ordinary differential equations, Eq. (4.1), where A and E are the concentrations of activated Sar1 and Sec proteins, respectively, and A^{max} and E^{max} are the maximum bound concentration of Sar1 and Sec in a particle. The k_M are the Michaelis Menten constants.

$$\begin{aligned} \frac{dA}{dt} &= k_0 \cdot \frac{A^{max} - A}{A^{max}} + k_1 \cdot A \cdot \frac{A^{max} - A}{A^{max} - A + k_{M2}} - k_2 \cdot E \frac{A}{A + k_{M1}} - \frac{A}{\gamma_1} \\ \frac{dE}{dt} &= k_3 \cdot A \cdot \frac{E^{max} - E}{E^{max} - E + k_{M3}} - \frac{E}{\gamma_2} \end{aligned} \tag{4.1}$$

The first term in $\frac{dA}{dt}$ is the external input with the rate k_0, which has the unit: $\frac{A}{s}$, Sar1 concentration per second. $A^{max} - A$ is the concentration of inactive Sar1 protein and is the substrate in the Michaelis Menten kinetics. k_0 is the only parameter that is not constant in time. It varies in time as a soft step function starting at 0 and ending at 1 Eq. (4.2). This is to avoid too drastic changes in the model when the input is applied. t is the time spent since the simulation started, h is the hill coefficient of the curve and is set to $h = 2$, and t_0 defines the time where $k_0 = 0.5$ which was set to $t_0 = 2$ s.

$$k_0 = \frac{t^h}{t^h + t_0^h} \tag{4.2}$$

The second term is the positive feedback loop with the rate k_1 with units $\frac{1}{s}$. Also here, the substrate is the concentration of inactive Sar1, $A^{max} - A$, and the rate is proportional with the concentration of active Sar1, A. Since it is a positive link it has a positive sign in front.

The third term is Sec inhibiting Sar1, hence the sign in front is negative. The rate is k_2 with the unit $\frac{1}{s}$. Here the substrate is A, and the rate in front is proportional with the concentration of Sec, E.

The last term in $\frac{dA}{dt}$ is the basal removal and therefore also has a negative sign in front. Here A is the substrate. From Michaelis Menten kinetics this should give an expression of the form $k_4 \cdot E^T \frac{A}{A+k_{M4}}$, but the enzyme, E, is assumed to be far from its saturation regime. The enzyme is saturated when k_M is much smaller than the substrate, A. In the limit $k_M \ll A$ the basal removal becomes: $k_4 \cdot E^T$, which is independent of the amount of the substrate.Far away from $k_M \ll A$ is when $k_{M4} \gg A$. Here, the basal removal becomes $k_4 \frac{A}{M4}$ and when collecting the constants into one constant we get: $\gamma_1 = \frac{k_{M4}}{k_4}$ the final expression for the term is $\frac{A}{\gamma_1}$.

The first term in $\frac{dE}{dt}$ is the positive link from Sar1 on Sec with the rate k_3 with the unit $\frac{1}{s}$. The rate is proportional with the concentration of active Sar1, A. The substrate is the concentration of inactive Sec proteins, $E^{max} - E$.

The second term is the basal removal, which is simplified in the same way as the basal removal of Sar1.

The sum of the active and the inactive proteins are assumed to be constant in time over the area that the particle span, and for Sar1 this can be written

$$a^{Total} = a^{inactive} + a^{active} = \text{constant}, \tag{4.3}$$

where a refers to the actual amount of Sar1. Dividing through with a^{Total} gives

$$1 = \frac{a^{inactive}}{a^{Total}} + \frac{a^{active}}{a^{Total}} = A^{inactive} + A^{active}, \tag{4.4}$$

where A^{active} elsewhere is referred to as A. The maximum amount of active protein, A^{max}, is when the amount of inactive Sar1 is zero, which means that $A^{max} = 1$. This also applies for Sec where the total maximum amount of bound Sec, $E^{max} = 1$.

4.2 The Spatiotemporal Regulatory Network

For Sar1 to be able to spread in space, Sar1 must be spatial dependent. In this model, the spatial spread happens through the positive feedback loop, since it is assumed that the process of recruitment of Sar1 is faster than the diffusion of Sar1 on the membrane. When new Sar1 is recruited it can not be situated exactly where the old one is bound, so it does make sense that this process is spatial dependent. The spatial dependence is so that the Sar1 concentration in one particle upregulate the Sar1 concentration in its neighbours. This leads to the spatiotemporal network seen in Figure 4.2. Here the oval circles represent one particle in our model. Because several Sar1 could attach within

one particle, there should also have been a positive feedback loop from the Sar1 in one particle to itself, but these are left out to simplify the drawing. The rates are written along the interaction lines. The input, k_0, is only applied to a particle in the center of the sheet, and is there to start the chain reaction of high concentration of Sar1 moving out through the sheet. The concentration of Sec, on the other hand, only reacts to the Sar1 concentration in its own particle. The basal removal is still present but not illustrated.

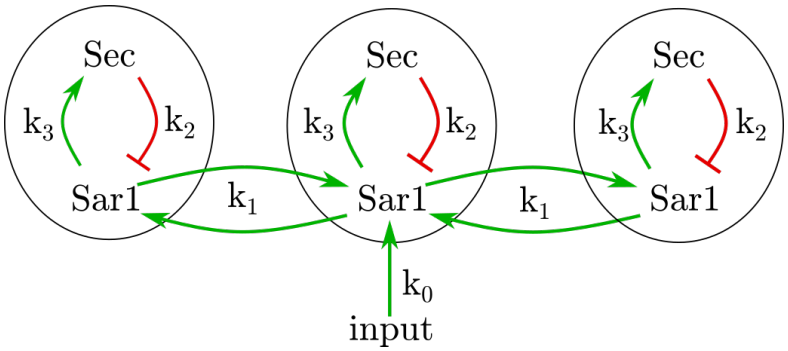

Figure 4.2: Spatiotemporal regulatory network. Each oval circle represents one particle. One particle in the center has an input signal. From here, the Sar1 concentration spreads to their neighbours. Basal removal is present but not illustrated.

Based on the spatiotemporal regulatory network (Figure 4.2) and again with the method of Michaelis Menten kinetics, we write up the changes in active membrane-bound Sar1 and Sec Eq. (4.5). Each particle is assigned a concentration of Sar1 and Sec and the protein concentrations in particle i are therefore denoted A_i and E_i.

$$\frac{dA_i}{dt} = k_0 \cdot \frac{A_i^{max} - A_i}{A_i^{max} - A_i + k_{M0}} + \sum_j k_1 \cdot A_j \cdot \frac{A_i^{max} - A_i}{A_i^{max} - A_i + k_{M2}} - k_2 \cdot E_i \frac{A_i}{A_i + k_{M1}} - \frac{A_i}{\gamma_1}$$

$$\frac{dE_i}{dt} = k_3 \cdot A_i \cdot \frac{E_i^{max} - E_i}{E_i^{max} - E_i + k_{M3}} - \frac{E_i}{\gamma_2} \tag{4.5}$$

The first term in $\frac{dA_i}{dt}$ is the external input to the system, which is only nonzero for the central particle in the middle of the sheet, but besides of that, it is unchanged from Eq. (4.1).

The second term is now a sum over the positive link from the particle itself and to its nearest neighbours. But simulations presented in this thesis have mistakenly only summed over the positive links from neighbours excluding the positive feedback loop on itself. A simulation have afterwards been run to test the behaviour of the system when the term from the positive feedback loop on itself is added. The behaviour of this system resembled what is presented in this thesis. For all these positive links, the

substrate is the concentration of inactive Sar1 in particle i: $A_i^{max} - A_i$ and the rate, k_1, is proportional with the concentration of Sar1 in the j-particles.

The third term and last term is unchanged from the single particle case Eq. (4.1) where Sec inhibiting Sar1 and the basal removal of Sar1 respectively.

The expression of $\frac{dE_i}{dt}$ is also unchanged from the single particle case, Eq. 4.1.

The parameters of the model will be specified in next section. But here we explain how the γ_1 and γ_2 are determined. This is done with considerations of having a model where cargo is present so vesicles are more likely to form. The half time of the turnover of Sar1, Sec23 and Sec24 in the presence of cargo are 1.1 ± 0.1, 3.7 ± 0.3, and 3.9 ± 0.3 respectively [8]. We work with Sar1 and Sec, and the relation in the half time of the turnover for these two is then around 1:4. The turnover rate is the rate at which new proteins attach to the membrane, but often this demands that old proteins detach. When the concentration of bound proteins is in steady state the rate of detaching is as big as the rate of attaching. Assuming that these measurements are made in steady state we implement the relation between the turnover rates for Sar1 and Sec by having the same relation between the half times in the basal removal for Sar1 and Sec: $\gamma_1 = 1$ and $\gamma_2 = 4$. The removal of Sar1 proteins do not only depend on basal removal, but when Sec is low it does. Since we wanted the 1:4-relation to also be present when Sec is low, the relation was implemented in the basal removal rates.

In this project we investigate if this simple version of the regulatory network is enough to replicate COPII vesicle formation.

4.3 Spatiotemporal Protein Dynamics on Flat Sheet of Particles

Now that the regulatory network in Figure 4.2 has been translated into the differential equations 4.5 we next wanted to test how these equations make the protein concentrations vary in time. We did that on a flat sheet of particles without updating neither position nor polarity vectors of the particles, emulating a flat ER membrane that can not bend. The simulation (Figure 4.3) shows that high concentration of active Sar1 spreads as a circle over the membrane emerging from one point.

As can be seen in Figure 4.3c and 4.3d, the center particles do not get red again but rather orange, meaning that the concentration of Sar1 does not fall back to the level where it started. This is because adaptation is not perfect. This is also seen in Figure 4.4 A), B), C), where the Sar1 concentration as a function of time is plotted for 5 particles in the center, 5 a little further out and 5 even further out (for more exact positions see inset). The non-perfect adaptation is well seen when looking at the central particles, where the concentration does not go to zero again after reaching maximum. In the biological system Sec is expected to completely deactivate Sar1, this is not happening completely here. The simulation is obtained with the parameters in Table 4.1. Here γ_1 and γ_2 is based on FRAP experiments at single ERES [8].

To be sure that the system can represent the adaptive behaviour of the biological system, a better adaptation was sought. A better adaptation was obtained when increas-

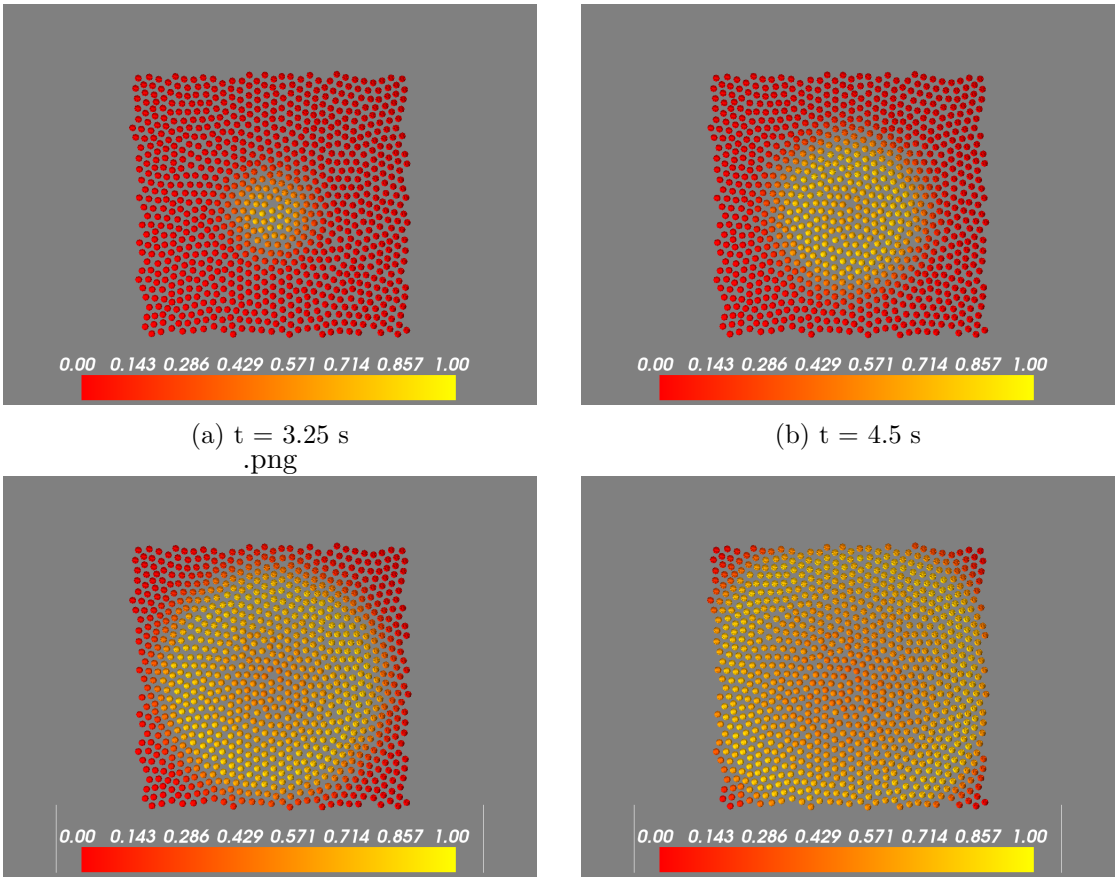

(a) t = 3.25 s
.png

(b) t = 4.5 s

(c) t = 5.75 s

(d) t = 7 s

Figure 4.3: The spreading of Sar1. Yellow indicate high concentration of Sar1. Red indicates low conentration of Sar1. (a): First high concentrations of Sar1 forms a circle. (b), (c), (d): Then it forms a ring, because the concentration of Sec-proteins has increased in the middle, which deactivates Sar1.

ing, k_1, which would increase the inhibition from Sec on Sar1. But if it was increased too much, rapid oscillations in the Sar1 concentration appear after the peak, which would make it impossible to classify the Sar1 concentration as an excitable medium, since it would not have a long refractory period after its excitation [15]. An intermediate k_1 with good adaptation and without the oscillating behavior of Sar1 was found at $k_1 = 20$.

But when $k_1 = 20$ the Sar1 concentration did not reach as high a maximum as before. Actually so low that it was thought to be problematic for vesicle formation. Therefore $k_1 = 3$ is kept for many simulations, even though other modifications may have made vesicle formation possible when $k_1 = 20$.

In the modelling process the lack of complete adaptation has not been problematic, because of how the coupling between protein dynamics and the bending of the membrane has been done. Exactly how, will be described in next section 4.4.

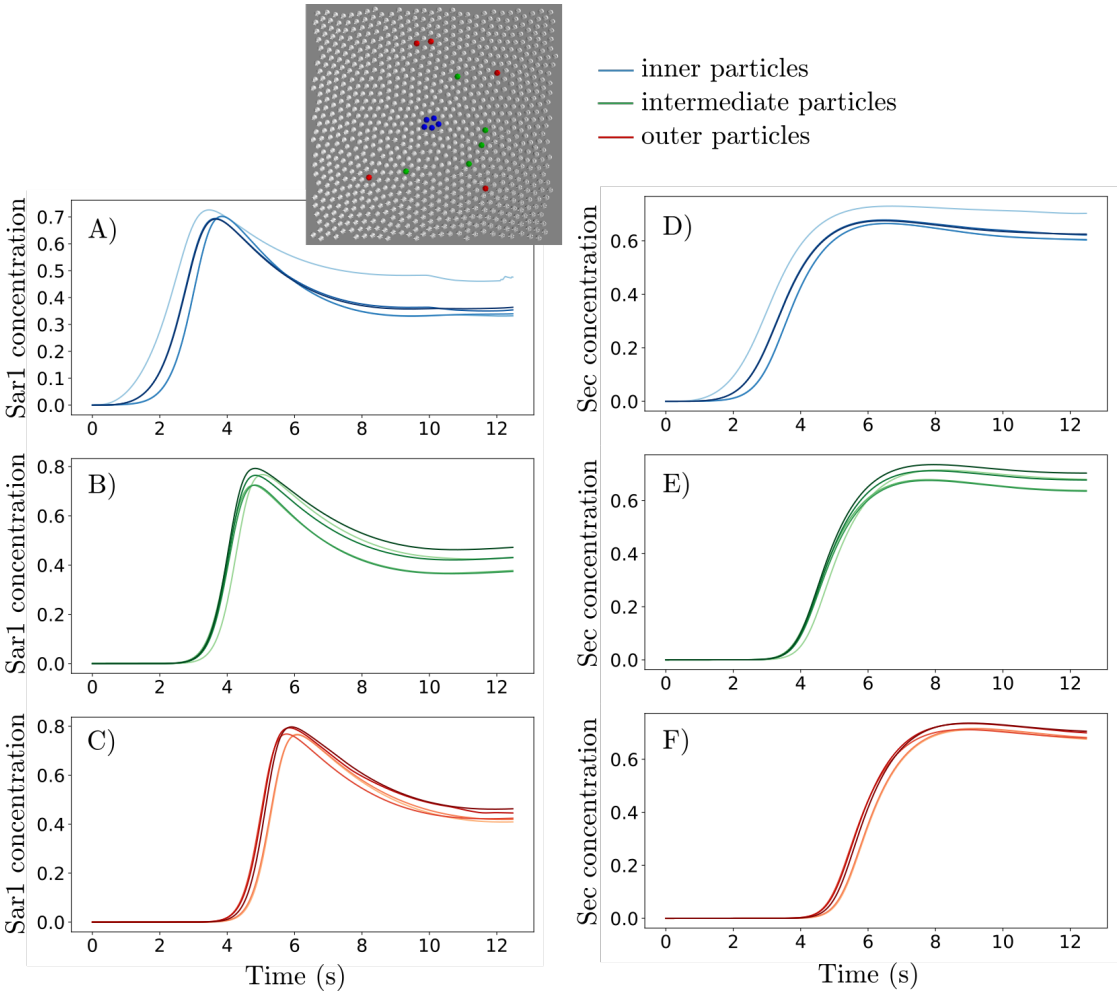

Figure 4.4: Spread of high concentrations of Sar1 and Sec from the inner particles (blue), through the intermediary particles (green), to the outer particles (red). The inset shows the placement of the particles that are monitored. A) - C) Sar1 concentrations as a function of time. Sar1 shows some but not complete adaptation. D) - F) Sec concentration as a function of time. Sec peaks after Sar1 has peaked and is the one deactivating Sar1.

In this section it is seen that Sar1 spreads in a ring formation, which Sar1 was proposed to do by [23]. We also see that Sar1 behaves like an excitable medium. The parameter, k_1, can be increased to obtain even better adaptation than seen in the figures in this section.

$$k_{M1} = k_{M2} = k_{M3} = k_{M4} = 0.5$$
$$max(k_0) = 1, \quad k_1 = 3, \quad k_2 = k_4 = 1$$
$$A_i^{max} = E_i^{max} = 1$$
$$\gamma_1 = 1, \gamma_1 = 4$$
timestep size: $dt = 0.025$,

Table 4.1: Parameters used for the model of protein dynamics in simulation in Figure 4.3. These parameters will be used for later simulations when protein dynamics is included until section 4.9

4.4 General Parameter Settings When Coupling the Protein Dynamics to the Membrane Bending Model

After having a model for the protein dynamics, the next question is: how to make the parameters, that control the bending of the sheet dependent on protein dynamics?

In section 2.2 I described how Sar1 initiates membrane curvature, while Sec23/24 and Sec13/31 also contributed to or stabilized this membrane curvature. In this model, Sar1 initiates the membrane bend, α, by setting α equal to the Sar1 concentration, A, with the linear relation $\alpha = A$. But this is only until Sar1 reaches its maximum, afterwards the α is fixed at the maximum Sar1 value, which resembles the curvature stabilization caused by Sec.

Making the simple relation $\alpha = A$ seemed reasonable because A, being a concentration, by definition runs between 0 and 1 (but practically between 0 and some value between 0 and 1) and that α had broad but reasonable variety of angles in the range 0 to 1 that corresponds to angles between 0 and 90 degrees. That the α is actually linear proportional to A is not necessarily true.

The curvature stabilization, that α stays up when A decreases, is thought to be caused by Sec, but in our model it happens automatically and independently of the actual concentration of Sec. The validation for doing this is that Sec does increase when Sar1 decreases (Figure 4.4) and does the job of curvature stabilization, whatever the specific value of Sec is.

In the following sections spherical and cylindrical symmetry are going to be mentioned, and to repeat what kind of parameter settings these symmetries implies the following Table 4.2 is reprinted.

Simulations always start with the particles being on a flat sheet with the AB-vectors, $\hat{p}$, parallel and pointing upwards perpendicular to the plane of the sheet. The starting positions of PCP will be specified in each simulation, unless $\lambda_2 = 0$, because that means that PCP has no influence on the mechanics of the sheet of particles.

Gaussian noise with maximum size of 0.05 was applied to each x-, y-, z-component of the positional vector, $\hat{r}$, the AB polarity vector, $\hat{p}$, and to the PCP vector, $\hat{q}$, if the

The symmetry ...	**... is obtained by having the settings:**
Spherical	Isotropic membrane bend. No PCP: $\lambda_1 = 1$, $\lambda_2 = 0$.
Cylindrical	Anisotropic membrane bend. PCP in circular pattern, $\lambda_1 = \lambda_2 = 0.5$.

Table 4.2: The needed settings to obtain the two symmetries: spherical and cylindrical.

PCP-vector was not fixed. The noise was scaled to the size of the time step multiplying it by $\sqrt{dt}$, so the size of the noise would be unchanged if dt is changed. dt should be squared because standard deviations add in quadrature.

The size of the time steps used in all simulations are $dt = 0.025$.

These settings are summed up in Table 4.3 and will be used for the results in the following sections unless something else is stated.

$\alpha = A$
The sheet starts being flat.
$\hat{p}$ starts perpendicular to sheet plane.
Gaussian noise of 0.05 on $\hat{r}$, $\hat{p}$, and $\hat{q}$.
Size of time steps: 0.025

Table 4.3: General parameter settings.

4.5 Vesicle Formation Only Using Isotropic Membrane Bending

Research simulating viral budding has succeeded to model the budding process by only using isotropic bending [17]. Isotropic bending is the key setting for spherical symmetry and since many COPII vesicles are spherical. Only using isotropic bending would also be a simple model. This suggestive model structure lead us to the following sub-question of the first question asked in the introduction about how to obtain vesicle formation within our models:

Can our model produce spherical vesicles by only using isotropic bending?

Vesicle formation with isotropic bending was investigated in two ways, with and without dependence of the protein concentrations.

The protein dependent simulation had α induce isotropic curvature still in the relation $\alpha = A$. It resulted in a bud going out of the sheet, but the budding vesicle then stopped growing outwards and increased in diameter instead, which means that the shape of the budding vesicle never got a bottle neck-shape nor left the membrane.

This could be because the protein dynamics was too fast compared to the sheet mechanics. Maybe the time scale separation (section 3.3) should be increased? But when would I know that it was increased enough to reject the model of only isotropic bending? Instead of increasing the timescale separation, the following more conceptual model independent of protein concentrations was tried out.

For the protein independent simulation (Figure 4.5) particles within a circle of radius 10 had the bending, α, fixed to 0.5 corresponding to an angle of 53° (yellow particles). Particles outside of that circle had $\alpha = 0$ (red particles).

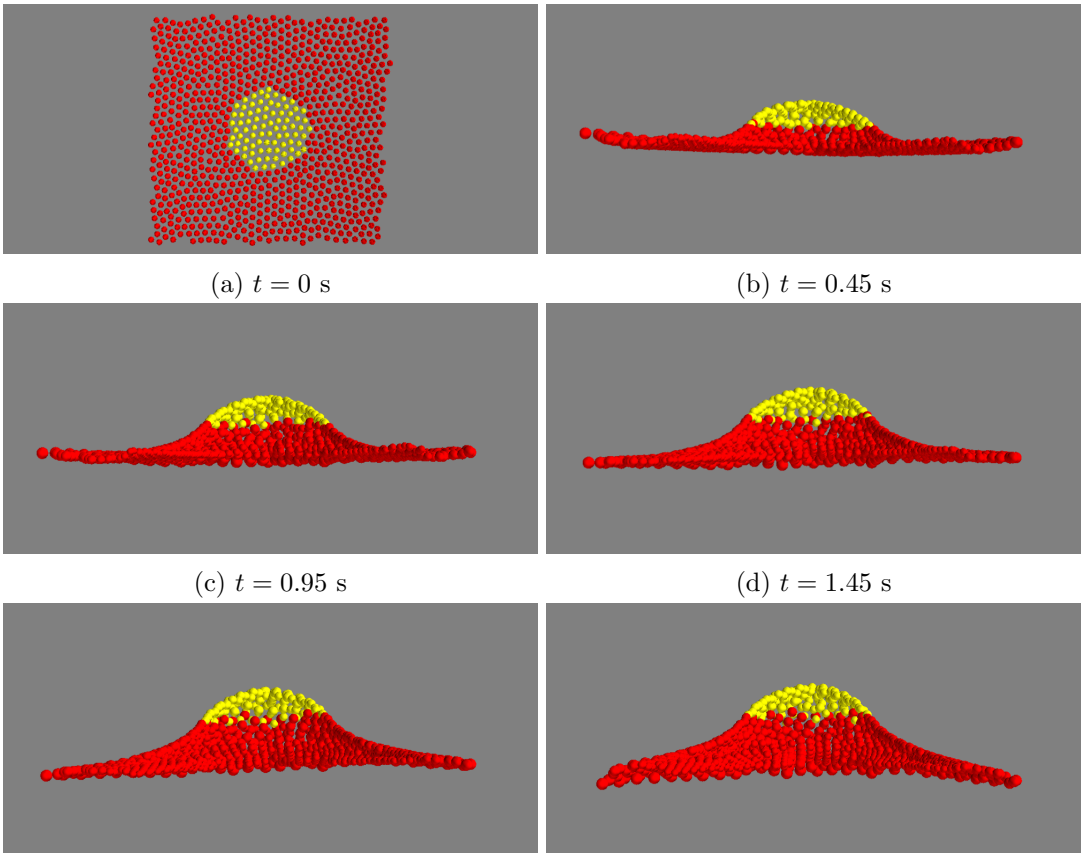

(a) $t = 0$ s (b) $t = 0.45$ s

(c) $t = 0.95$ s (d) $t = 1.45$ s

(e) $t = 1.95$ s (f) $t = 2.45$ s

Figure 4.5: Simulation with isotropic positive bending. Yellow particles have $\alpha = 0.5$, red particles have $\alpha = 0$.

The simulation resulted in a bud that grew fast at first but then grew slower and

slower. This bud never got a bottle neck and was not close to budding off. The time span of the simulation was increased several times to check if a bottle neck arose at a later time. But the yellow particles with the bend does not change their shape much after time $t = 0.45\ s$. After that time only red particles rose a little. Whether the slow changes would lead to a bottle neck some time in the future can not be rejected, but it is found unlikely. We also find it unlikely that vesicle budding would slow more and more down like this because it seems unfavourable for the transport efficiency.

To form a ring of particles, the optimal number of particles is 7, when the angle between each particle is 53°. From the start there are around 9 particles along the diameter of yellow particles, so the area should be large enough for vesicles to form.

An idea to get closer to vesicle formation while having only isotropic bending was to use of negative isotropic bending in a ring around particles with positive bend. But at the COPII vesicle formation, no proteins are observed to induce negative curvature [13]. Therefore this idea was discarded.

Another idea was that the bottle neck did not form because the sheet is too rigid. A way to relax the membrane tension could be to lower λ_1 or to change the way the nearest neighbour is defined. Instead of using the Voronoi diagram the nearest neighbours could be defined by being particles within a certain distance. These ideas have not been further investigated.

isotropic α	$\alpha = 0.5,\ r < 10$ $\alpha = 0,\ r > 10$
$\lambda_1 = 1,\ \lambda_2 = 0$	for all particles

Table 4.4: Used parameters when investigating vesicle formation using only isotropic bending (Figure 4.5).

Using the parameters in Table 4.4, it is not possible to form a vesicle by only applying isotropic positive bending. Since there is also evidence that vesicles are not only spherical (section 2.2.4), the approach using only isotropic is not further investigated.

4.6 Sar1 and Anisotropic Bending

Constitutively active Sar1 is experimentally observed to induce the tubular behaviour [4], [7] (section 2.2.4). Tubes have cylindrical symmetry and as explained in section 2.4.3 this model demands anisotropic bending to make cylindrical symmetry. We therefore hypothesize that Sar1 bends the sheet anisotropically. But how can Sar1 do that? When looking at the particle in the top of Figure 2.14 C Sar1 should bend the membrane in one direction but not the other, but how this is possible, is a little hard to imagine when looking at Figure 2.3b. Another reshape Sar1 could perform is an elongation (Figure 4.6 C). Here the particle in A would make a flat sheet, and the particle in B would make isotropic bending, and the particle in C would make anisotropic bending according to

the following explanation.

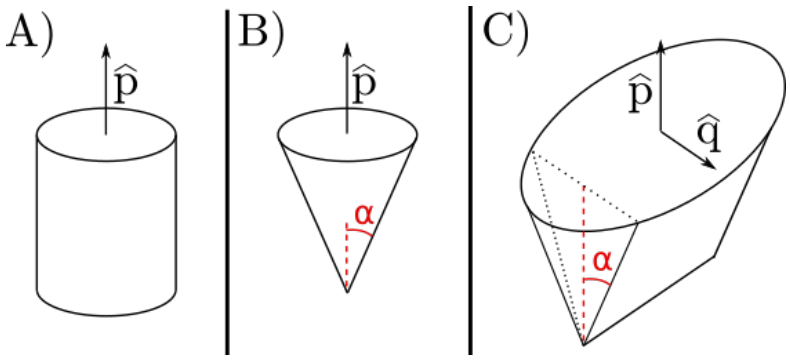

Figure 4.6: Three shapes of particles. A) A sheet of these particles would create a flat sheet. B) These particles would produce isotropic bending. C) These particles would produce anisotropic bending.

When elongated curve-inducing particles pack tightly and in an ordered manner on the ER membrane, the particles would be able to pack more tightly in one direction than the other. This would make the curvature higher in the direction where they can pack most tightly. This is illustrated in Figure 4.7, where tightly packed elongated particles are seen from the top. The PCP-vector can be interpreted as this elongation and is illustrated as the arrows inside the particles. In this model, PCP points in the direction where the sheet is bend most strongly, which would be the direction where the particle is shortest. To match this explanation with anisotropic bending, the thought about higher curvature in one direction than the other is taken to the extreme, in the sense that one direction is assigned no bending at all while other directions do prefer bending of the ER membrane.

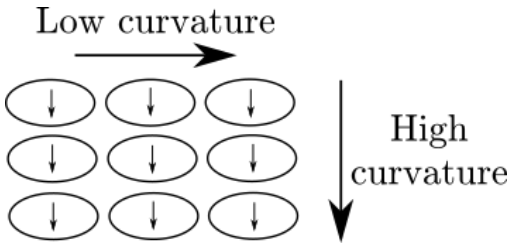

Figure 4.7: Elongated particles packed tightly and ordered would curve the membrane more in one direction than the other. The arrows inside the particles are PCP-vectors.

But when looking at the crystal structure of Sar1 in Figure 2.5, Sar1 alone looks pretty round and not elongated. Still some other protein could regulate how Sar1 binds to the ER membrane, such that Sar1 gets a certain pattern with more distance to each other in one direction that the other, which would effectively work as the elongation would.

Here a suggestive explanation on how Sar1 could cause anisotropy is presented, but exactly how the crystal structure of Sar1 is related to anisotropy is beyond the scope of this thesis.

4.7 Vesicle Formation Using Isotropic and Anisotropic Membrane Bending

In the next three subsections we will test the hypothesis that Sar1 bends the membrane anisotropically while Sec creates isotropic membrane bending:

Can we produce spherical vesicles as well as tubes using both isotropic and anisotropic bending?

In the first subsection, spherical vesicle formation will be investigated without dependence on protein concentration and in the second subsection, spherical vesicle formation is driven by protein dynamics. This two step process is done in the case simulations do not produce good results. Then it should be clearer whether the problems come from the concept of modelling the system with the two kinds of membrane bending or come from the coupling of our two models. In the third subsection tube formation will be investigated.

4.7.1 Vesicle Budding Independent of Protein Dynamics

To investigate the concept of having two regions with different membrane bending, we must identify where these regions should be defined on the sheet, so they resemble the regions when defined by protein concentration. On Figure 4.8 the expected shapes through the budding process are seen along with the expected placement of high Sar1 concentration giving anisotropic bending (red) and high Sec concentration giving isotropic bending (yellow). In A) only Sar1 has increased in concentration and initiates the anisotropic bending. Later in B) and C) Sar1 has recruited Sec in the central particles, and thereby there is only a ring with anisotropic bending at the border of the budding vesicle.

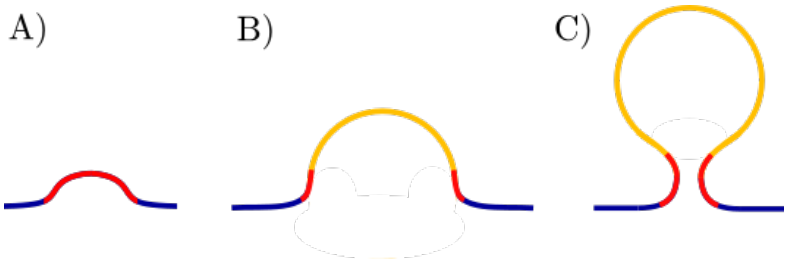

Figure 4.8: Expected states of the vesicles formation. High Sar1 concentration (red) gives cylindrical symmetry. High Sec concentration (yellow) gives particles spherical symmetry. No bound COPII proteins (blue) give no bending.

Based on these budding states, the simulation starts out with the settings (Figure 4.9a) where a circular area with the radius of 10 of the models spatial units have anisotropic bending. PCP is fixed in a circular pattern. Together this gives cylindrical symmetry (red area). Particles in the blue area prefer no bending. Later (Figure 4.9b), when particles moves out of the plane, particles farther away from the sheet than a certain distance of 5 get isotropic bending which gives them spherical symmetry (yellow area).

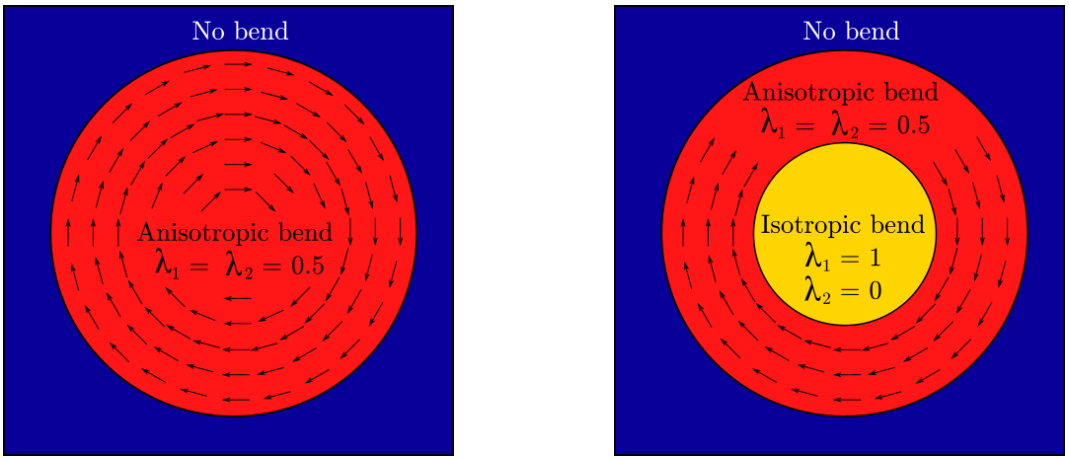

(a) (b)

Figure 4.9: Parameter settings for simulation in Figure 4.10. Sheet is seen from above. Arrows are PCP. Settings in red areas give particles cylindrical symmetry. Settings in the yellow area give particles spherical symmetry. (a) Initial settings. (b) Later settings when the vesicle starts budding.

The settings in Figure 4.9 made the simulation in Figure 4.10. This simulation shows a budding vesicle that forms with the contours of a bottle neck with cylindrical symmetry (red) and a ball shaped bud on top with spherical symmetry (yellow). Even though the bottle neck is not so narrow and the vesicle seems far from budding off the results look promising. Instead of investigating what makes the bottle neck narrower in this scenario we rather wanted to investigate such things in a membrane bending model coupled to protein dynamics. For now we conclude that simulations using only positive α and both isotropic and anisotropic bending seem promising for simulating the budding process.

4.7.2 Vesicle Budding Driven by Dynamics of Sar1-Sec Regulatory Network

The next step is to make the bending of the sheet dependent on the protein concentrations. This is done much as I described in section 4.4, but the new important addition is that Sar1 and Sec cause different kinds of bending. In section 2.2.4 and 2.4.3 I argued that Sar1 generates anisotropic bending and also causes PCP to organize in a circular pattern, which together gives cylindrical symmetry. Sec, or more specifically Sec13/31,

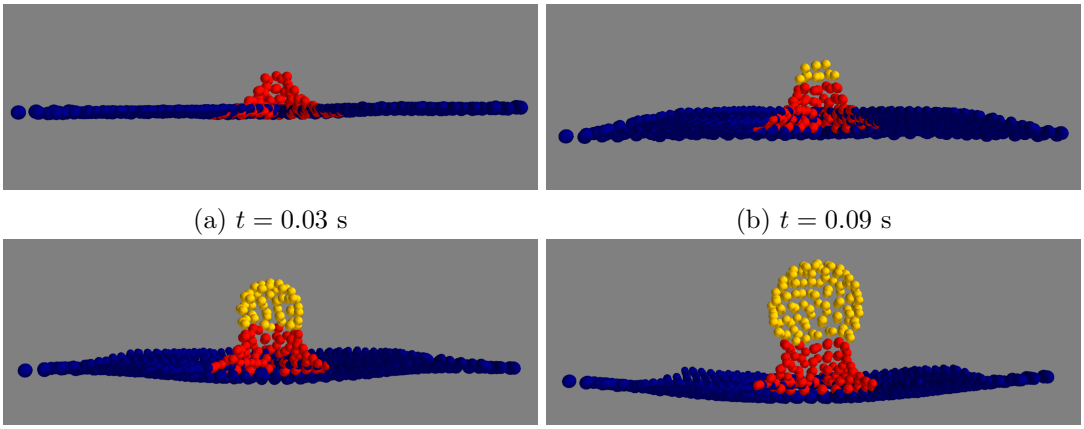

(a) $t = 0.03$ s (b) $t = 0.09$ s

(c) $t = 0.3$ s (d) $t = 1.2$ s

Figure 4.10: A simulation where the bend of the membrane is independent of protein dynamics. Blue Particles prefer no bending. Red particles have settings leading to cylindrical symmetry. Yellow particles have settings leading to spherical symmetry.

leads to spherical symmetry (section 2.2.2). This change from anisotropic to isotropic bend is modelled by having a limit, E_{lim}, that when the concentration of Sec exceeds E_{lim} the bend becomes isotropic. We tried out different values for E_{lim} and chose one that made the simulation create vesicles.

The settings in Table 4.5 gave the simulation in Figure 4.11. Here, red particles have $E < E_{lim}$ which means that the particles make anisotropic membrane bending, and yellow particles have $E > E_{lim}$ and make isotropic membrane bending. A snapshot on how the protein concentration has spread at time $t = 3$ s is seen in Figure 4.12.

anisotropic α, $\lambda_1 = \lambda_2 = 0.5$	when $E < E_{lim}$
isotropic α, $\lambda_1 = 1$, $\lambda_2 = 0$	when $E > E_{lim}$
$E_{lim} = 0.4$	
PCP fixed in circular pattern	
Number of intermediary time steps: 500	
The input k_0 is applied in 6 central particles	
Other parameters related to the regulatory network are identical to the ones in Table 4.1	

Table 4.5: Parameters used for vesicle formation driven by protein dynamics (Figure 4.11).

This result has a narrower bottle neck than before the membrane bending was coupled to protein dynamics. Further more the vesicle leaves the membrane as seen in Figure

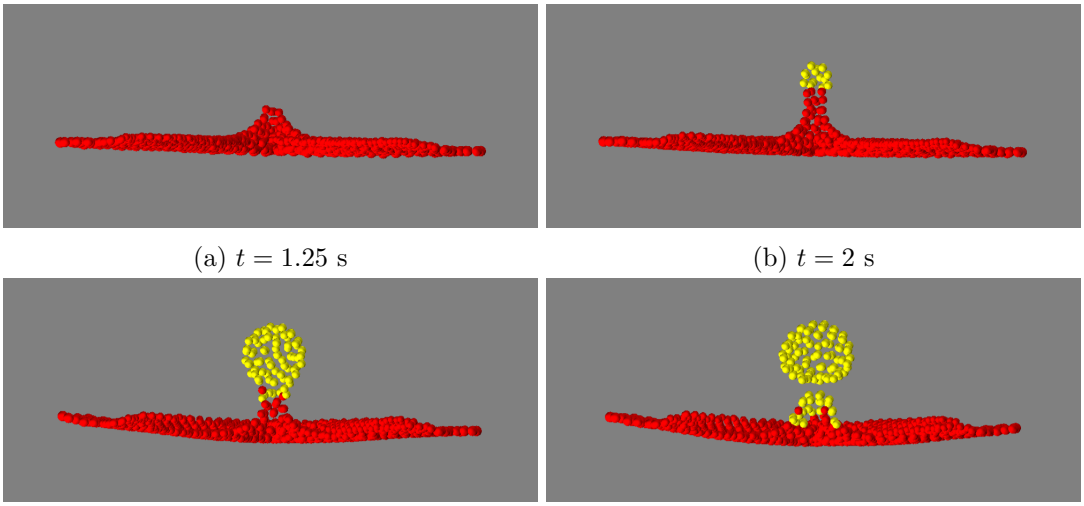

(a) $t = 1.25$ s (b) $t = 2$ s

(c) $t = 3$ s (d) $t = 3.275$ s

Figure 4.11: Vesicle formation driven by protein dynamics. Red particles have $E < E_{lim}$ leading to cylindrical symmetry. Yellow particles have $E > E_{lim}$ leading to spherical symmetry.

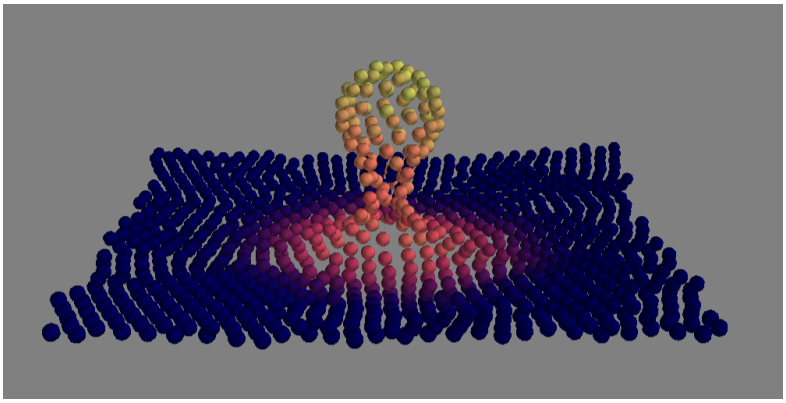

Figure 4.12: Protein concentration during vesicle formation at $t = 3$. Blue particles have low Sar1 and Sec concentrations. Red particles have high Sar1 but low Sec concentration. Yellow particles have high Sec concentration.

4.11d. This is a surprisingly good result, and what caused the budding off will be further discussed in the end of this thesis.

These investigations show that it is possible to model a budding vesicle only using positive membrane curvature, by having a spherical and a cylindrical region that is regulated from protein dynamics. This model also captures the vesicle leaving the membrane.

4.7.3 Tube Formation

In experiments it is observed that when an always-active mutant of Sar1 is applied to liposomes as the only COPII protein, tubes are formed [4], [7], [2]. So how should the model be modified to reproduce these results?

An idea could be to remove Sec from the model. Then there is nothing besides of the basal removal to inhibit Sar1, and Sar1 would probably reach a higher maximum concentration. By removing Sec, the bend will never become isotropic, and will therefore never have spherical symmetry.

But for the simulation in this section (Figure 4.13) it is done by setting limit, E_{lim} so high that the Sec concentration could never reach it. E_{lim} is the limit where Sec turns the symmetry of the particle into spherical symmetry. This modification will also cause particles to keep their anisotropic bend and never get isotropic bending, leading to spherical symmetry. But the maximum size of the bend will not increase as if Sec was not there. Instead the maximum concentration of the mutant of Sar1 would be the same as when modelling the non mutated type of Sar1. But this is expected to be less important.

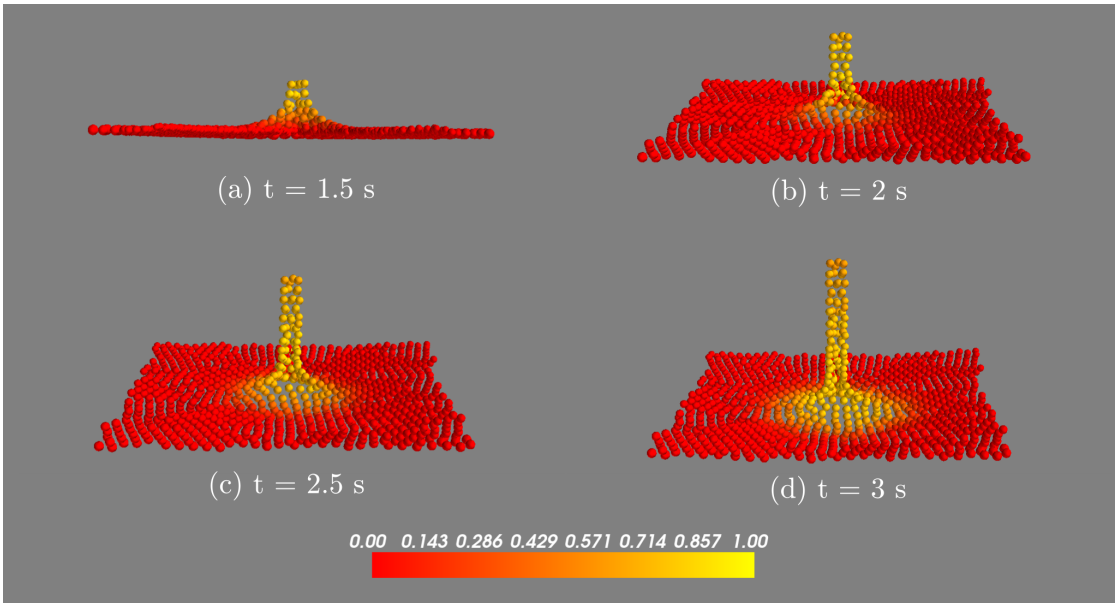

Figure 4.13: A mutant of Sar1 that can not be deactivated is modelled. This forms a tube. The color illustrates the concentration of Sar1.

$E_{lim} = 1$
Other parameters are identical to Table 4.5

Table 4.6: Parameters used for simulating the mutant of Sar1 (Figure 4.13)

The simulation (Figure 4.13) has the settings in Table 4.6 and makes a tube that grows and grows in length. In the experimental data in Figure 2.7, some tubes are still connected to the liposomes and other leaves the membrane as tubular vesicles. The tubular vesicle leaving the membrane has not been further investigated in this project. The tubes in the experimental data are also not straight as in the current simulation. The simulation makes the straight tube because the PCP is fixed. Maybe if the PCP was able to vary more the tubes would also not be as straight.

From this simulation we conclude that we succeeded to model the mutant of Sar1 that produce tubes. Together with the result in previous sections we conclude that the model, using two symmetry regimes, that is driven by the dynamics of Sar1 and Sec, is able to reproduce both the tube formation caused by the Sar1 mutant, and normal COPII vesicles formation.

4.8 Budding with PCP Self-organizing in a Circular Pattern

Previous results had PCP fixed in the circular pattern needed to do cylindrical symmetry. In the real system this pattern is likely to emerge as a result of the interaction between particles. This leads us to the question:

What kind of interaction will make PCP organize in a circular pattern?

In this section we will first present a modification to the particle interaction that should be able to make PCP organize in circular pattern, next we give a possible biological interpretation of this modification. Then the question about whether the modification achieved its goal is investigated in two steps: Can the modification make PCP stay in a circular pattern when first organized that way? And can the modification make PCP self-organize into circular patterns when starting from random oriented order? Lastly vesicle formation with self-organizing PCP will be investigated.

4.8.1 Modifying the Particle Interaction to Obtain Self-organizing PCP

For the sheet to form a cylinder, PCP must be organized in a circular pattern as described in section 2.4.3. But if PCP was initialized into a circular pattern and was allowed to move according to the interaction in S_2, Eq. (2.3), PCP will reorganize and orient themselves parallel to each other.

When we want the circular pattern to be stable we can modify the interaction such that an angle between PCP vectors is favoured. A favoured angle, β, between neighbouring PCP-vectors, can be applied in kind of the same way as α is applied between AB-polarity vectors described in section 2.4.2. But β should not be applied between every neighbouring pair. This can be seen when looking at the PCP in a cylinder (Figure 2.16) where the PCP-pairs along cylinder's axis are parallel. It is also illustrated in Figure 4.14 where the pair of PCP in the red ring is parallel while the pair in the blue ring has an angle between them.

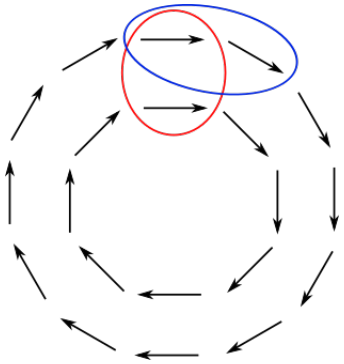

Figure 4.14: An optimal configuration of PCP for the formation of cylinders from a flat sheet. The neighbors in the red ring have no angle between their PCP vectors. The neighbors in the blue ring have an angle between their PCP vectors.

The pair of PCP vectors in the blue ring can be identified as having their PCP parallel to the directional vector between them. This is used when applying the favoured angle between the right pairs of PCP, as is done when redefining the PCP, $\hat{q}$ in Eq. (4.6).

$$\hat{\tilde{q}}_i = \frac{\hat{q}_i + \beta(\hat{q}_i \cdot \hat{r}_{ij})(\hat{p}_i \times \hat{q}_i)}{|\hat{q}_i + \beta(\hat{q}_i \cdot \hat{r}_{ij})(\hat{p}_i \times \hat{q}_i)|} \tag{4.6}$$

The factor $(\hat{q}_i \cdot \hat{r}_{ij})$ determines how big the angle between neighbouring $\hat{q}$s should be in the range $0 - \beta$. If the PCP vectors are parallel to the directional vector, $\hat{r}_{ij}$, between them, the angle becomes the maximal size of β (red ring Figure 4.14). If $\hat{q}$s are perpendicular to $\hat{r}$ the angle becomes zero (blue ring Figure 4.14). The cross product $(\hat{p}_i \times \hat{q}_i)$ determines the direction of the correction and will thus be perpendicular to both $\hat{p}$ and $\hat{q}$.

4.8.2 Possible Biological Interpretation of β

How can β be interpreted? One way is to look at β as a shape modifier. This is along the earlier interpretation of α, where α is interpreted as modifying the shape of the particle to become cone shaped instead of cylindrical (4.15 A and B). C and illustrates the elongation of the particle that happens when PCP is applied. As explained in section 4.6 the elongation would mean that the particles can not pack equally dense in both directions on the ER membrane and cause anisotropic bending, which is depicted in lower row in Figure 4.15.

The angle β can be interpreted as a wedge-shape along the sheet plane. The idea is that this would cause the particles to organize into the wanted circular pattern as illustrated in the bottom part of D in Figure 4.15. Still after reaching the circular pattern in PCP on a flat sheet some frustration would be present because particles in circles further out do not require as high a β as particles in the inner circles. But in the end what is wanted is that particles are placed in a cylinder, where all particles requires the same β.

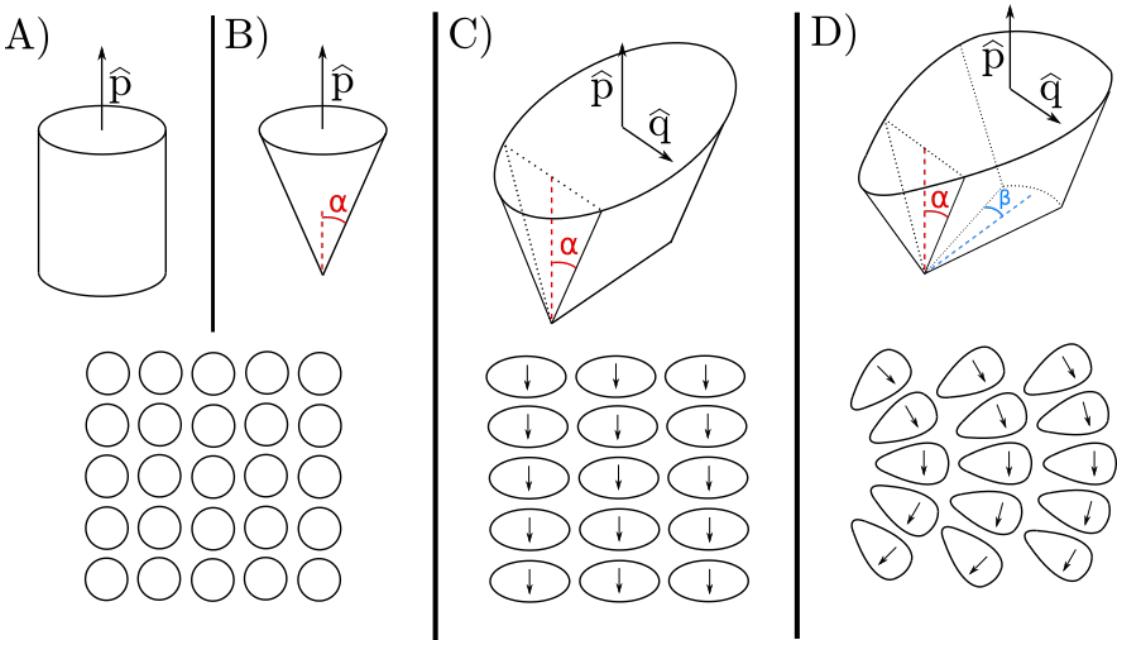

Figure 4.15: The shapes of the particles cause them to organize in different patterns. A) This particle does not bend the membrane. B) This particle bends the membrane isotropically. Both A) and B) make the particles organize with the same density in all directions (lower panel of figures) C) This particle makes anisotropic bending and can organize more compactly in one direction than the other. D) This particle makes anisotropic bending and can organize most compactly along a circular line.

A suggestion in this thesis is that Sar1 is responsible for the change in shape of a particle from A to D in Figure 4.15. While Sec is responsible for changing the shape from D to B. How Sar1 is responsible for the changes in the shape of a membrane particle is still up for discussion and beyond the scope of my thesis.

4.8.3 Keeping the Circular Formation in PCP

Having defined the new particle interaction I wanted to first test whether PCP, organized in a circular formation, will be stable, i.e. remain in the circular formation.

The simulation in Figure 4.16 shows that the β-implementation was enough for PCP to stay in circular pattern. The simulation is based on the settings in Table 4.7.

PCP vectors start in a mathematical defined circular pattern, Eq. (2.8).
PCP is updated according to Eq. (2.5).
$\beta = 0.2$
The input k_0 is applied in the 1 central particle.
Other parameters are identical to Table 4.5

Table 4.7: Parameters used when testing whether the implementation of β can keep PCP vectors in circular formation (Figure 4.16).

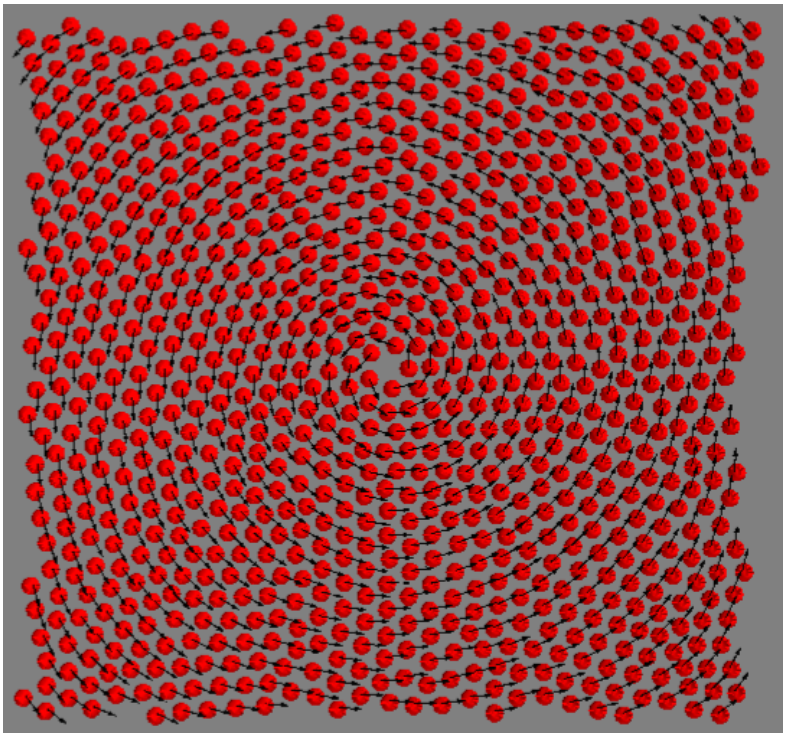

Figure 4.16: PCP vectors stay organized in a circular pattern when β is implemented. The black arrows represent PCP. $t = 2.5s$. $25,000$ updates of PCP have been done and PCP is still organized in the circular pattern.

4.8.4 Spontaneously Emerging Circular Pattern in PCP

Having shown that PCP stays in a circular formation when initialized in this pattern, we wanted to test if the circular formation can emerge if PCP vectors are initialized to point in random directions along the sheet plane.

This was more problematic to obtain and new questions arose. It turned out to be dependent on the initial random orientation. Therefore spontaneous circular formation

in PCP was attempted by using three different procedures.

Each procedure was evaluated by running the simulation a number of times with different random seeds, differing the random starting position of the PCP-vectors and the noise applied to position, AB-polarity and PCP, and then counting how often the PCP vectors formed a circular pattern.

In all of the three procedures α was set to 0, which means that the sheet will keep being flat. The organization of PCP as well as the membrane bending are properties of Sar1, that the PCP formation happens before the membrane bending is achievable if membrane bending depends sigmoidally of Sar1 (Figure 4.17). The organization of PCP seen in this section can then happen while the Sar1 concentration is at a low level where the bend is still insignificant (red ring in Figure 4.17). For simplicity, instead of implementing this nonlinearity as a sigmoidal, we have implemented it in two discrete steps. First step where no protein kinetics are applied while PCP organize in a circular pattern. Second step where the protein kinetics and their influence on α and the lambda settings are applied. This section describes the first step.

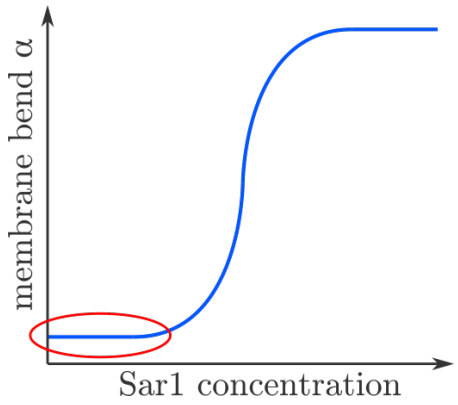

Figure 4.17: A sigmoidally dependence between the membrane bend and the Sar1 concentration. This relation can validate that the circular organization of PCP can happen before the membrane starts bending.

Procedure 1

First we tried to let the PCP follow the spreading of Sar1, such that when Sar1 increased above a certain limit in a particle, the particle would get PCP assigned by setting its $\lambda_1 = \lambda_2 = 0.5$.

We fix $\lambda_1 = 1$, and $\lambda_2 = 0$ for the central particle with the input of the protein kinetics. This corresponds to removing its PCP vector. We do this because a particle, surrounded by particles that have their PCP pointing circular around it, will have the frustration that no PCP-direction is better than another. Then we thought it was better to leave it out and avoid that the PCP of the central particle disturbs the PCP of the particles around it.

The first particles with PCP assigned will be the particles in a ring around the central particle with the input, unless noise in the system has moved them around. We wanted to check if the circular PCP formation could happen already in this first ring of particles with assigned PCP, and the simulation was stopped short after PCP spread to particles farther out.

From the start the ring of particles around the central input particle consisted of 6 particles. The β that such 6 particles would prefer for PCP to form a circle is $\beta = 0.58$. Therefore this β was tried out by running the simulation with 20 different random seeds. Neither of these turned into a circular formation.

Also $\beta = 0.4$ was tried, which corresponds to 7-8 particles having their PCP in a circle. The same 20 random seeds was used. Also neither of these resulted in a circular PCP formation.

The number of intermediary time steps between the updates of the protein kinetics was increased from 500 to 750 in these simulations. This was done to be more sure that the PCP had time to find a steady state before further protein updates.

From these results we conclude that the possibility for PCP forming a circular pattern in a 6-particle ring is less than 5% within the settings in Table 4.8. This was at first a bit disappointing, because we expected PCP to be a property of Sar1 which in this model spreads out from a single point. But maybe the circular formation first emerges when Sar1 has spread over a bigger area? This is what procedure 2 and 3 investigates.

PCP starts randomly oriented in the sheet plane.	
Number of intermediary time steps: 1500	
$\beta = 0.4$	$\beta = 0.58$
Other parameters are identical to Table 4.7	

Table 4.8: Parameters used for investigating procedure 1.

Procedure 2 and 3

Procedure 2 and 3 are independent of the protein dynamics. They investigate what sizes of areas PCP will spontaneously organize into circular patterns. In procedure 2 only particles within a certain radius from the center of the sheet were assigned PCP while in procedure 3 all particles where assigned PCP. Procedure 2 then takes the shape of the spreading Sar1 into account and also that the PCP organization may happen when Sar1 has not spread to as big an area as in procedure 3.

The PCP formation is evaluated after 20,000 updates of PCP, which corresponds to 0.5 s. It turned out that the formation was not just circular or not circular, often a spiral emerged that resembled the circular behavior far away from the center, but at the center PCP pointed in a radial direction. A circular PCP orientation for procedure 3 can be seen in Figure 4.18a while a radial behavior can be seen in Figure 4.18b. Since it

is exactly the central particles that have to have PCP in a circular pattern to produce a tube going out of the plane, this distinction is very important.

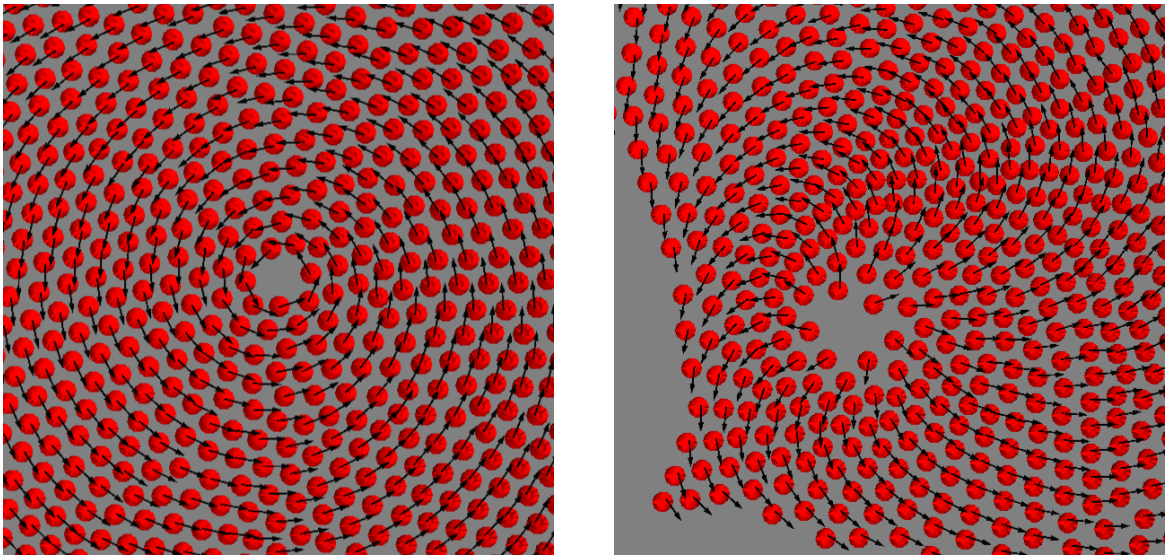

(a) (b)

Figure 4.18: Resulting PCP formations when using procedure 3. (a) A PCP formation that is also circular at the center of the spiral, $\beta = 0.2$. (b) A spiral formation with PCP pointing radially in the center of the spiral, $\beta = 0.4$.

The success rate of circular formation for the different sizes of areas where PCP is assigned are found by running the same code but for 10 different random seeds (Table 4.9). The column 'Formation of spirals' counts how many simulations obtained a spiral independent of the orientation of the particles in the center of the vortex. The column 'Circular in the center' only counts the spirals with circular PCP orientation for the central particles.

From Table 4.9 we conclude that the bigger the area that PCP can organize within, the bigger is the chance that a circular formation will occur.

When comparing the two sets of simulation for procedure 3 with two different sizes of β, it looks like smaller β makes forming of spirals form less likely. What seems more clear is that bigger β make the PCP more radial in the center.

When looking at procedure 2, one could get the idea that PCP becomes more radial when the area is increased. Here the statistics are probably too low to be sure. But it does make sense that frustration occurs in a big circular pattern, where all particles have the same β, because there are more particles in an outer ring in the circular pattern than a more central ring. The angle between each pair of PCP does not need to be as high in the outer ring as for the particles in a smaller more central ring. The unnecessary big β for PCP in outer particles presses the bend radial in for the PCP in the inner particles. Examples of the spirals for the different areas sizes are seen in Figure 4.19. A

Procedure	Area with PCP assigned	β	Formation of spirals	Circular in the center
2	circle $r = 6$	0.4	2/10	2/2
2	circle $r = 10$	0.4	0/10	0/0
2	circle $r = 12$	0.4	3/10	2/3
2	circle $r = 18$	0.4	6/10	1/6
3	entire sheet (square)	0.2	8/10	8/8
3	entire sheet (square)	0.4	10/10	0/10

Table 4.9: Success rate of circular formations after $t = 0.5$ s starting from randomly oriented PCP. r is the radius of the circle where PCP is applied. r is in the model's spatial units. Simulations are independent of protein dynamics, this table contains the parameter settings used.

solution to this radial problem for bigger areas, could be to make β variable throughout the circles. Maybe the size of β could dependent on the protein kinetics. But this has not been prioritized to try out.

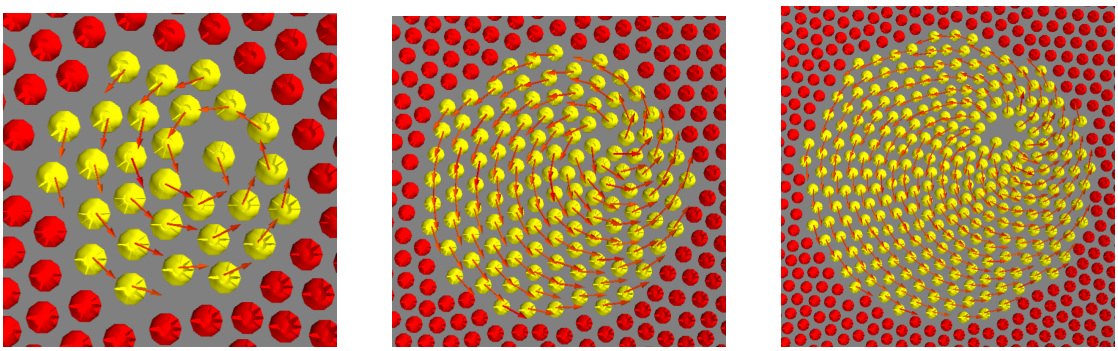

(a) Procedure 2 $r = 6$ (b) Procedure 2 $r = 12$. (c) Procedure 2 $r = 18$.

Figure 4.19: When the area, where PCP vectors organize within, gets bigger, it seems more likely that radial behavior occurs in the center of spiralling formations.

From these investigations we conclude that spontaneous circular formation does occur with our β-implementation in Eq. (4.6). It also looks like the area of particles with PCP assigned needs to have a certain size before the circular formations form spontaneously. But to avoid radial behavior in the center of the circle, β must probably be lowered as the area increases in size. The most optimal configuration tried in this section was by using procedure 3 where the entire sheet has PCP assigned and $\beta = 0.2$.

Comparing Energies of Different PCP Formations

Because the optimal circular formation was so rarely occurring, see Table 4.9, we wanted to verify that the circular formation was a global minimum.

To investigate this, 20 simulations with different random seeds were run. Procedure 2, described in section 4.8.4, was used with a radius of 15 in units of the model. The energy of the end configuration was calculated as the potential, see Eq. (2.1), and the potential for a given formation was defined from a mean over the last 20 saved configurations with the uncertainty defined from the standard deviation: $\sqrt{\frac{1}{N}\sum_{i=1}^{N}(x_i - \bar{x})^2}$. For each simulation it was made sure that it had reached steady state by monitoring that the potential was oscillating around some constant potential. The final formation is separated in three different types of PCP formations. The optimal circular spiral formation (Figure 4.20a), the radial spiral formation (Figure 4.20b), and the also often seen bending formation that did not close into a circle (Figure 4.20c. The results are seen in Figure 4.20d, where the energies of the system are grouped by color after the three observed formations.

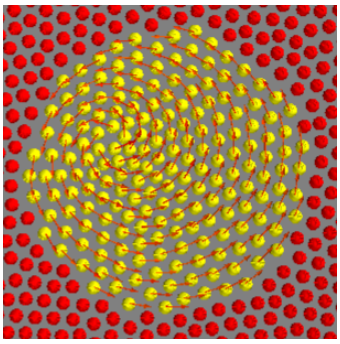

(a) Circular spiral.

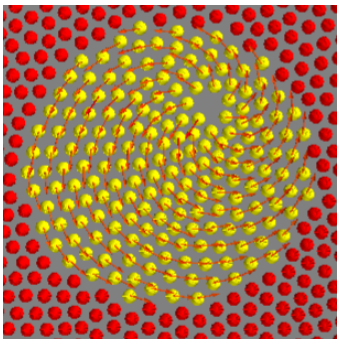

(b) Radial spiral.

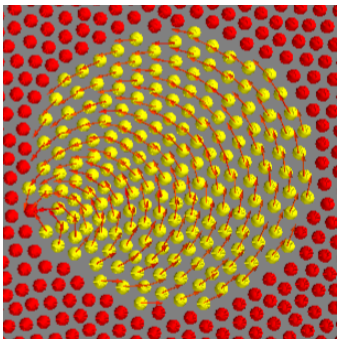

(c) Bending formation.

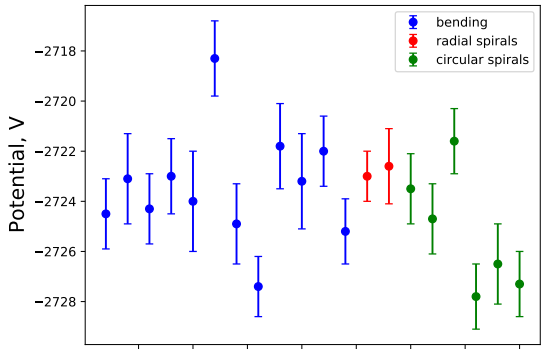

(d)

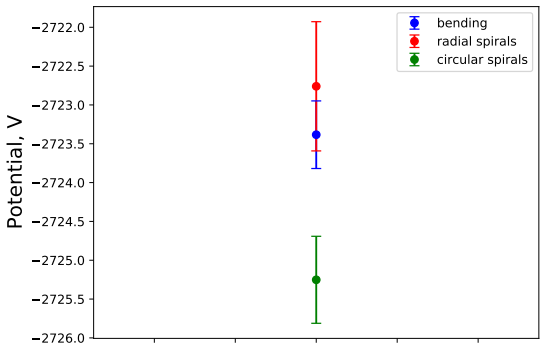

(e)

Figure 4.20: (a)-(c) Three different types of resulting formations. (d) Simulation runs with different random seeds. For each simulation the potential of the system's end configuration is calculated as an average of the last 20 iterations. (e) Weighted averages of the potentials of each type of PCP-formations in (d).

From the means in 4.20d a weighted average, $\bar{x}_w = \frac{\sum_i x_i/\sigma_i^2}{\sum_i 1/\sigma_i^2}$, is calculated for each type of formation together with its uncertainty, $\sigma' = \sqrt{\frac{1}{\sum_i \frac{1}{\sigma_i^2}}}$. These are seen in Figure 4.20e.

In Figure 4.20d it looks like most of the energies lie within each other's uncertainties and therefore can not be distinguished, which can explain why the simulation quite often does not form into the preferred circular spiral. In Figure 4.20e it becomes visible that the preferred circular spiral is actually the energy statre of all the formations. This validates the chosen math applied when implementing an angle to the PCP vectors. But the potential energy of the circular formation is only 0.07% smaller than the energy of the bending formation. Therefore it is understandable that the simulation does not always end in the preferred global minimum.

4.8.5 Forming Vesicles from Spontaneously Formed PCP-circles

After achieving a spontaneously formed circular formation, whose center particle also stays in the circular pattern, this data can be used as the starting configuration for a simulation, where the membrane bending is driven by protein dynamics while PCP is free to move according to Eq. (2.5). Will this simulation keep the PCP in circular formation in a way where a cylinder can form?

Which particle to infer the input is decided from finding the particles with maximum vorticity. The vorticity, ω, is a measure of how much circulation in the xy-plane, which is also the sheet plane, the neighbouring particles' PCP vectors have. The vorticity is calculated as seen in Eq. (4.7), where j indexes neighbouring particles and N is the number of voronoi neighbours a given particle has. The x and y superscript indicate that it is the x- or y-component of the vector. The difference inside the sum can be identified as the z-component of the cross product between the directional vector between two neighbouring particles, $\hat{r}_{ij}$, and the PCP-vector, $\hat{p}$. The vorticity can only be calculated this way as long as the sheet is in the xy-plane, therefore it is only calculated in the beginning of the simulation where particles are in the xy-plane.

$$\omega = \frac{1}{N}\sum_{j}^{N}\left|\hat{r}_{ij}^{x}\hat{q}_{j}^{y} - \hat{r}_{ij}^{y}\hat{q}_{j}^{x}\right| \tag{4.7}$$

The settings in Table 4.10 gave the result in Figure 4.21. As can be seen, vesicle formation is succeeded while coupling membrane bending to protein dynamics while PCP is updated. This means that our implementation of β in Eq. (4.6) is sufficient to obtain self-organizing PCP formations that can lead to vesicle formation. The conditions for spontaneously formed circular patterns in PCP can probably be optimized further.

Again we have the success of a vesicle leaving the membrane. According to these simulations the budding process takes a couple of seconds, for this one specifically around 3.5 s. Now it should be possible to model the entire process from spontaneously forming a circular pattern in PCP to vesicle formation in one simulation. This should be possible by letting the bend, α, depend sigmoidally of the Sar1 concentration as described in section

4.8.4. But because of time limitation this have not been attempted. With a working model for vesicle formation all kinds of questions could be asked and investigated, what we have focused on, is how different amount of cargo proteins affect the vesicle formation.

Starts from a spontaneously formed circular PCP formation (procedure 3).
$\beta = 0.2$
Number of intermediary time steps: 500
Other parameters are identical to Table 4.7

Table 4.10: Parameters used for simulating vesicle formation after implementing β (Figure 4.21f).

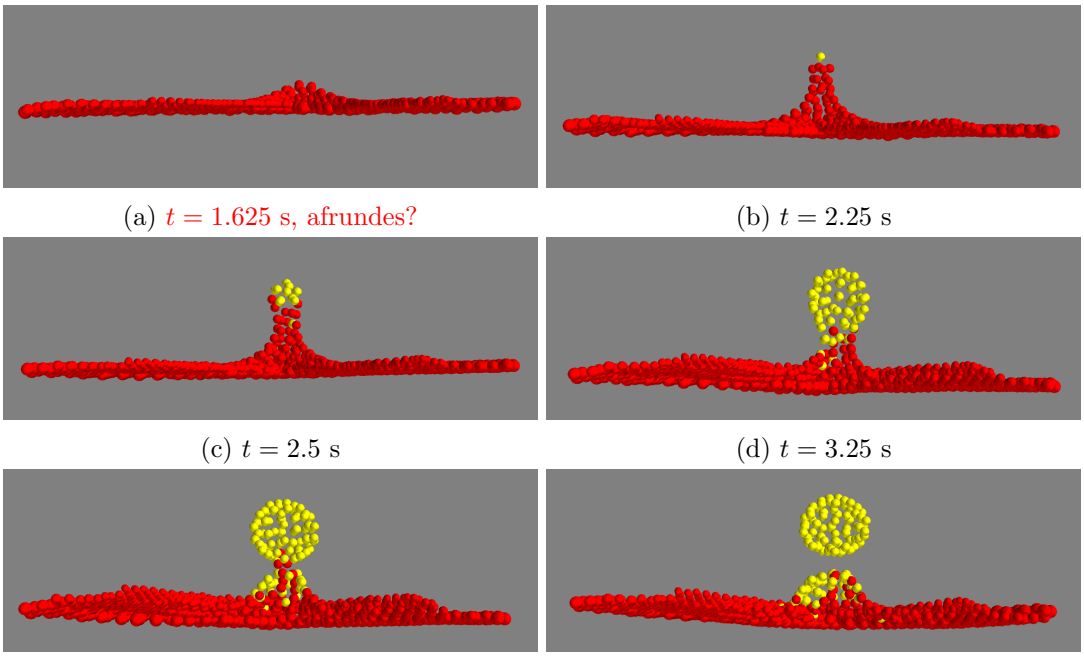

(a) $t = 1.625$ s, afrundes?

(b) $t = 2.25$ s

(c) $t = 2.5$ s

(d) $t = 3.25$ s

(e) $t = 3.5$ s

(f) $t = 3.75$ s

Figure 4.21: Vesicle formation driven by protein dynamics. The circular PCP formation have formed spontaneously and PCP keeps getting updated according to Eq. (2.5) through out the simulation. Red particles have $E < E_{lim}$ leading to cylindrical symmetry. Yellow particles have $E > E_{lim}$ leading to spherical symmetry.

4.9 The Role of Cargo

Now that we are able to produce vesicles, we wanted to know how the cargo proteins affect the vesicle formation. The amount of cargo protein influences the dynamics of the COPII protein concentrations. It also influences the angles between the hinges of the Sec13/31-rods. That makes it possible for the outer vesicle coat to adopt various sizes and geometries (see section 2.3). This leads us to investigate the last question mentioned in the Introduction:

How does cargo influence the vesicle size?

Increasing the cargo load changes the turnover rate of Sar1 and Sec (section 2.3). In section (section 4.2) we argued that the half time of the turnover corresponds to the half time parameters in the basal removal for Sar1 and Sec. So when cargo changes, so should the half times of the basal removal. But if we change these half times of the basal removal without changing other rates we would change the steady states of the system. We wanted to change the dynamics of the way to steady state, but without changing the steady state. This was done by multiplying the entire rates of Sar1 or Sec by a factor.

Seeing how the turnover rate changed without and with cargo in section 2.3 the factor for Sar1 should be proportional to the amount of cargo and for Sec it should be inverse proportional to the amount of cargo, Eq. (4.8)). Here, $\frac{dA_i^c}{dt}$ and $\frac{dE_i^c}{dt}$ is the change in Sar1 and Sec concentrations when cargo is implemented, k_i^c is a constant proportional to the amount of cargo, and $\frac{dA_i}{dt}$ and $\frac{dE_i}{dt}$ is the changes seen in Eq. (4.5) before cargo was implemented, i indexes the different particles.

$$\begin{aligned} \frac{dA_i^c}{dt} &= k_i^c \frac{dA_i}{dt} \\ \frac{dE_i^c}{dt} &= \frac{1}{k_i^c} \frac{dE_i}{dt} \end{aligned} \tag{4.8}$$

Maybe this is actually a better interpretation of how cargo influences the turnover rate than only changing the removal rate, because probably the turnover rate depends both on how quickly proteins leave the membrane, making space for new proteins to bind, and also on how quickly new particles bind.

The amount of cargo assigned to a particle, k_i^c, is specific for a specific particle i, which is set in the beginning of the simulation. The cargo is distributed over the sheet as a soft step-function dependent on the particle's distance to the center of the curl in PCP (Figure 4.22). This gives a circular area with high amount of cargo and low amount of cargo in the rest of the sheet. The expression for k_i^c is seen in Eq. (4.9), where d_i is each particle's distance from the center of the PCP-vortex, d_{lim} sets the radius of the circular area with high cargo concentration, and C_{top} sets the level of the high concentration within the circle. The hill coefficent, h, is set to 6, to get a transition between low and high concentrations of cargo that is both steep but still smooth. The smooth change in

cargo concentrations is necessary because the differential equations used in the numerical simulation become bad approximations when the changes suddenly become very big. After the cargo k_i^c is set according to Eq. (4.9) the lowest cargo concentrations is set to $k_i^c = 0.1$ to avoid dividing with zero in $\frac{dE_i^c}{dt}$ in Eq. (4.8).

$$k_i^c = \frac{d_{lim}^h}{d_i^h + d_{lim}^h} \cdot C_{top} \tag{4.9}$$

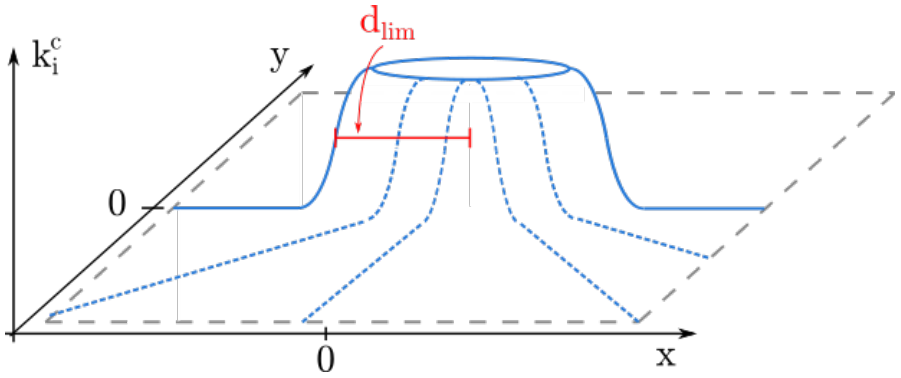

Figure 4.22: The cargo distribution over the sheet of particles.

Varying the amount of cargo was done in two ways. Either varying d_{lim}, the spread of the cargo, or varying C_{top}, the height of the distribution, leading to a higher concentration of cargo in the center. The results of these investigations are seen in Figure 4.23. The size of the vesicles are measured by finding the distance between the two particles with the most opposite pointing AB polarity-vectors in the xy-plane. The errorbars is obtained from running the simulation with 5 different random seeds for each measurement.

When varying the spread of the cargo, d_{lim} (Figure 4.23a), the cargo concentration was kept constant at $C_{top} = 4$. When varying the cargo concentration (Figure 4.23b) the spread of the cargo was kept constant at d_{lim}=10. Other parameters are found in Table 4.11.

A constant line is fitted to the data to check whether the variations in the vesicle size is only fluctuating around an otherwise constant vesicle size, when the cargo is increased. For the investigation about varying the radius of the spread of cargo (Figure 4.23a) a constant line had a p-value of $3.7 \cdot 10^{-12}$. When varying the concentration (Figure 4.23b) a constant line had the p-value of 0.0028. For both graphs the p-value is below the designated threshold of significance of 0.05, and we can reject that the variations in vesicle size is only caused by fluctuations.

A linear fit was also made, these had the p-values 0.77 for the data in Figure 4.23a and 0.81 for the data in Figure 4.23b. This means that it is likely that the vesicles grow in size as the amount of cargo is increased, both when "increased cargo" means that the cargo covers a bigger area and when it means that the concentration of cargo increases.

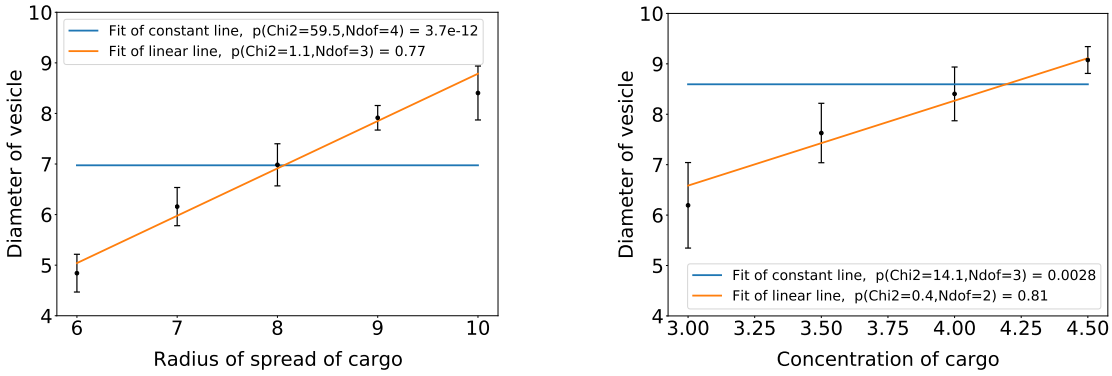

(a) (b)

Figure 4.23: Vesicle sizes obtained with different amounts of cargo. (a) One way to change the amount of cargo by changing the radius of the circular area where cargo is applied. (b) Another way to change the amount of cargo by changing the concentration of the cargo load on the same circular area of the sheet.

PCP vary according to Eq. (2.5)
PCP starts from circular formation obtained by Eq. (2.8)
$\beta = 0.2$
$k_0 = 20$
Elim $= 0.05$
Number of intermediary time steps: 1500
Other parameters regulating protein dynamics are identical to Table 4.1

Table 4.11: Parameters used for investigating how vesicle sizes depend on the amount of cargo (Figure 4.23).

4.9.1 The Amount of Cargo for Vesicle Formation

A broader range of measurements than those seen in Figure 4.23 were tried for both investigations, but the simulation did not produce nice vesicles when exceeding the ranges of the x-axes. In this subsection I explain what happens in the simulation when the amount of cargo gets too low or too high.

When the radius of the spread of the cargo was 5 or smaller, a bud as broad as the cargo distribution forms but without the constriction like a bottle neck and no vesicle leaves the membrane. This happens because not enough particles would get enough active Sar1 to form a tube and a budding vesicle.

When the radius of the spread of the cargo became larger that 10, the simulation often produced two vesicles right after each other. This could resemble something that

also happens within the cell, but the results could not be used to compare the sizes of the vesicles, since the size of one is distributed on two. Another observation was that few of the simulations ended by having a hole in the sheet after the vesicle left. We think this is caused by an acceleration in the spread of the protein concentration, such that the membrane bending process needs more time steps to adapt to the proteins concentration, but we did not have time to investigate this properly.

When understanding why the simulation does not form vesicles outside of the range plotted in Figure 4.23b it helps to look at the dynamic of Sar1 and Sec in a single particle when different amounts of cargo is applied (Figure 4.24). Here, it can be seen that higher concentrations of cargo delay the recruitment for Sec. This delay determines how long the tube gets before particles with isotropic bending emerge in the top. If Sar1 is quickly inhibited, as with low concentrations of cargo, a tube is not formed properly before isotropic bending shape the particles into a sphere, which means that no bottle neck arises. Instead the bud will grow in width until all particles with a proper amount of cargo are included into it, but no vesicle will form and detach. This is what is observed when the concentration of cargo gets down to 2.5 or lower.

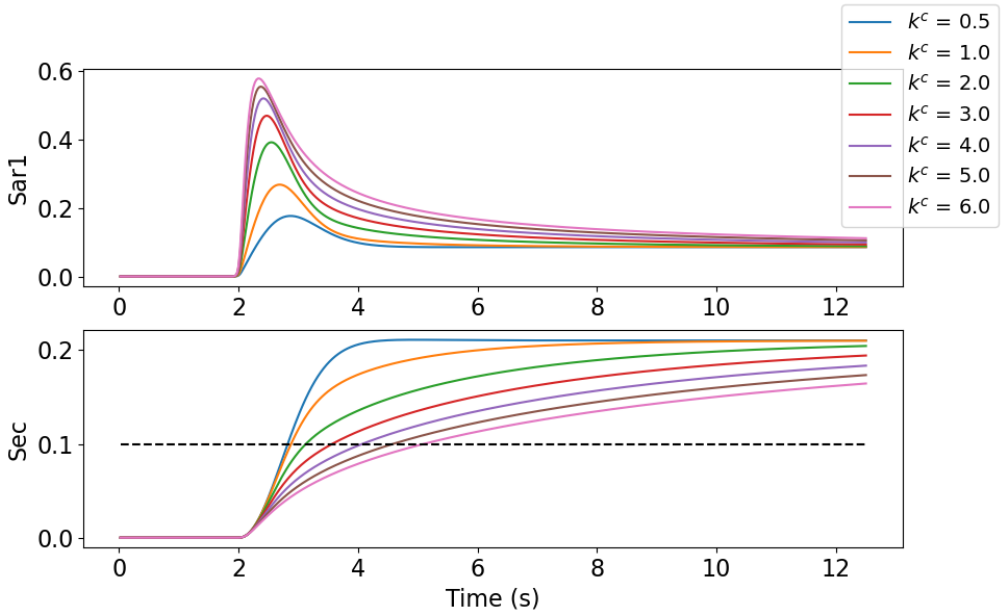

Figure 4.24: Protein dynamics in a single particle for different amounts of cargo, k^c. The dashed line marks the limit from where a particle would get isotropic bending. The higher the amount of cargo, the steeper is the increase in Sar1, but the slower is the descend of Sar1, which is caused by the delay in the upregulation of Sec.

If the concentration of cargo is increased too much, Sar1 is inhibited very slowly and a long tube forms before the spherical vesicle is formed on top. But the critical part is that the concentration of active Sar1 also becomes steeper and higher (Figure 4.24). This causes Sar1 to spread faster, where after Sec spreads equally fast. When

the Sec, and thereby the isotropic bending, spreads too fast the shape of the tube does not have time to change into a vesicle before the entire tube becomes isotropic. This results in the formation of several vesicles nearly at the same time. The fast spreading of Sar1 also seems to cause holes in the sheet plane, where Sar1 had spread to. We think this happens as an alternative way of fulfilling the preferred angle between particles, which is apparently faster than the process of tube formation. These problems were already observed for concentrations of 4.5, where extra simulations were run to obtain five measurements of the vesicle size. 60% of the simulations where discarded because they produced several vesicles and some also had the sheet torn apart.

4.9.2 The Size of a Particle

Now we have produced vesicles in various different sizes by applying different amounts of cargo. If we assume that we have covered the range of typical vesicle sizes: 60-100 nm, we can translate the model's spatial units into nm.

The smallest and largest of the averaged vesicle sizes in Figure 4.23 is 4.8 ± 0.4 and 9.1 ± 0.3 in the units of the model. Since we know that vesicles normally have the size of 60-100 nm, we are able to translate the spatial units of the model into nanometers. If we assume that we have covered the range of vesicle sizes that the model can produce we can find that 1 of the models spatial units is either $\frac{60\text{ nm}}{4.8} = 12.5$ nm when looking at the lower limit, while the upper limit gives $\frac{100\text{ nm}}{9.1} = 11.0$ nm. To get one translation factor we use the mean of these two values: 11.75 nm.

With this factor we can find the size of a particle. The particles are point particles with an equilibrium distance of 2 model units, which is 23.5 nm.

We can also find the size of the square sheet we have been working with to be 700 nm both in width and length. This fits well with the size of an ERES [11] [12].

5 Discussion and Conclusion

5.1 Question 1

How can we couple the model of protein dynamic to the model of membrane bending to replicate COPII vesicle formation?

Our Simple Regulatory Network

Since we are able to simulate vesicle formation with the simple network, it supports that we captured some essential mechanisms in the regulatory network of COPII proteins.

The vesicle formation could not have been done without the positive feedback on Sar1, which was somewhat debated in literature. That this model is able to form vesicles supports the existence of a positive feedback loop, possible through the protein Sec16 [26] or through the mechanism that Sar1 rather binds to areas with high curvature [10].

Only Isotropic Bending

We coupled this network to the bending of the ER-membrane. We wanted to do this by only using isotropic bending because [17] achieved this for viral vesicle formation. We could not achieve vesicle formation by only using isotropic bending.

Both systems only have membrane bending protein that perform positive membrane bending, therefore the bottle neck is expected to cost energy to produce. This is also the reason why they observe that the budding process develops slower and slower.

Maybe our system could also create a similar budding process if the membrane was less rigid? This could maybe be modelled by lowering λ_1 or by defining the neighbours of the particles differently.

Isotropic and Anisotropic Bending

We wanted a system that was able to reproduce both spherical vesicles and the tubular structures observed when Sar1 is constitutively active [4] [7]. This made us hypothesize that Sar1 bends the membrane anisotropically and also make the PCP vector in our model organize in a circular pattern, which is crucial in formation of tube structures. The spherical structures was then formed by Sec that made the bending become isotropic. Coupling the protein dynamics and the membrane bending this way we were able to reproduce vesicle formation.

We suggest that both these features of Sar1 are caused by the shape of a particle when the Sar1 concentration in that particle is high. If the particles are elongated and broader in one end than the other (Figure 4.15 D) it would lead to the features of anisotropic bending and PCP forming in a circular pattern. Since the reshaping of the particles happens when the Sar1 concentration is high, it would be obvious that it could be because of the shape of Sar1. But when looking at the crystal structure of Sar1 in Figure 2.5, the elongated shape do not seem very present. We also suggest that other

constrains could be present that would make Sar1 bind to the membrane in that same way as it would if it was caused by the suggested shape of Sar1. We have considered if it could be the shape of the Sar1-Sec23/24 complex that caused the anisotropy and the circular PCP formation. However since tubules are observed when only the constitutively active Sar1 is applied on liposomes, we rejected this idea. Perhaps this shape arises from the shape of the N-terminal helix that Sar1 inserts into the membrane or the way that it is inserted into the membrane? Exactly how to relate the anisotropy and the circular formation of PCP to the crystal structure of Sar1 will be out of scope of this thesis.

5.1.1 Extra Question for Question 1

We could not form vesicles using isotropic and anisotropic bending without having PCP organized in a circular pattern. Therefore we also needed to investigate:

How can PCP spontaneously organize in circular patterns?

We successfully implemented an angle, β, between PCP vectors such that they could retain a circular formation. This implementation was also able to spontaneously form circular PCP formation that were useful for creating vesicles in $\frac{8}{10}$ of the simulations. This was when the area of the PCP organization had a certain size and when β had a certain size that was calibrated to the size of the area of the PCP organization. In this case $\beta = 0.2$ and all particles of the particle sheet were part of the PCP organization.

Our optimal size of the area of PCP organization includes the entire sheet, which is 700 nm wide in each direction. This is on the size of ERES which is several hundred nanometres [11], or up to 800 nm [12]. Dependent on how many vesicles should be able to form from one ERES simultaneously it could be necessary to optimize our spontaneous PCP organization in smaller areas.

The Circular PCP Formations are the Lowest Energy State

Our difficulties of spontaneously forming the circular PCP formations made us ask if our implementation at all gave the circular formation a lower energy state compared to other resulting formations we saw. This investigation made us conclude that the circular formation had a lower energy state but we also saw that it was only 0.07 % smaller than the energy state of the formation that was closest in energy state to the circular formation. This explains our struggles but it also questions whether our implementation is the optimal one. From the fact that the circular pattern is a global minimum and that we achieved a success rate $\frac{8}{10}$ we would say that our implementation have promising utilization. Maybe even higher success rate than $\frac{8}{10}$ can be found if the relation between the size of the formation area and the size of β is further optimized?

Answer

With the membrane bending model driven by protein dynamics we achieved vesicle formation. This was achieved while the regulatory network of the protein dynamics was

strongly simplified. We had to assume that Sar1 bends the membrane anisotropically and also make PCP self-organize in circular patterns, while Sec stabilizes membrane curvature, but makes it isotropic.

5.2 Question 2

How can the COPII vesicle formation get a bottle neck and what causes the scission of the vesicle?

Since we have succeeded to simulate vesicle fission with our membrane bending model we can reply with the general answer: it is energetically favourable for the membrane to form a vesicle when exposed to the membrane bound COPII proteins.

But the bottle neck of the budding vesicle, which is the former state for vesicle fission, was only achieved with this model of energy minimization under the assumption that Sar1 bends the ER membrane anisotropically and make PCP organize in a circular formation.

When accepting these assumptions we can ask more detailed: what dynamics in our model cause the vesicle to leave the membrane? Here we observe that the line of division, between particles with isotropic bending (the yellow particles in Figure 4.21) and particles with anisotropic bending (red), moves down the bottle neck of the budding vesicle, meaning closer to the plane of the membrane. But what can explain this observation?

If we had built a model where the spread of the Sec concentration from particle to particle would catch up with the spread of the Sar1 concentration, this could explanation the observation. But in our model the Sec concentration only depends on the Sar1 concentration in that same particle. This makes it impossible for the spread of Sec to spread faster than Sar1.

When looking at the spread of Sar1 during the vesicle formation we see that it also spreads further and further out on sheet. This indicates that the time scale separation is not entirely at the limit where the membrane bending has reached steady state before the next protein update happens. If we had been in that limit, more of the particles with high Sar1 concentration on the sheet would instead have formed into a tube and not stayed on the sheet.

Vesicle Fission Happens Because of the Size of the Time Scale Separation

I wonder if the isotropic bending also moves down the bottle neck because the time scale separation is not as big as it could be. I imagine that if the membrane bending had more time before next protein update, new particles on the bottle neck that get isotropic bending would move to the vesicle instead of staying on the bottle neck. Then the isotropic bending would not move down the bottle neck and the vesicle would not leave the membrane. So does the vesicle fission only happen because the time scale separation is not in the limit where the bending of the membrane reaches steady state before next protein update?

I tried increasing the time scale separation with a factor of 4 (data not shown) and the vesicle size increased from 10.1 to 15.5 in spatial units of the model. This increase in vesicle size supports that the timescale separation plays a role in vesicle formation and separation. According to this theory of vesicle fission the vesicles got bigger because the time scale separation got bigger, which means that the bending of the membrane had more time to reorganize before the protein concentrations are updated. To really test this theory we have to go to the limit where the membrane reaches steady state before the protein concentrations are further updated. Here we should check if the vesicle would stay connected to the membrane and only grow in size as the protein concentrations spread. This might be done by increasing the time scale separation further, but this investigation could also be limited by computer power if the time scale separation has to become infinitely long.

So maybe our vesicle fission is only an effect of not having big enough time scale separation in our simulations. But could it be that this actually resembles what happens in the cell? Could the protein concentration spread faster than the ER membrane has time to rearrange?

Vesicle Fission Happens Independently of the Size of The Time Scale Separation

Even in the case where our simulations of vesicle fission is only an effect of too small time scale separation and does not resemble what happens at ER, I will argue that we still have simulations that would also make vesicle fission if we had big enough time scale separation. These are the simulations, where cargo is only applied in a certain area (section 4.9). Here the spread of Sar1 is stopped when it reaches particles within areas of low cargo concentration. This means that the spread of Sec can catch up with the spread of Sar1 and in the end make every particle in the budding vesicle and on the bottle neck specifically have isotropic bending, which would cause the vesicle to scission from the membrane. These simulations also have 3 times bigger time scale separation than previous simulations and still have vesicle fission.

Vesicle Fission Happens because the Right Vesicle Size is Obtained

Another theory of why the vesicle leaves the membrane is that it happens when the vesicle has reached a critical size. The isotropic particles on the vesicle bud all have a favoured angle. That angle corresponds to a favoured vesicle size. At some point the system does not go to a lower energy state by increasing the size of the vesicle. Then the theory is that at some point, it is just too costly for the system to increase the vesicle size and it is rather pinched off. To investigate this we could try different sizes of the maximum bend in the system. This could be done by changing the relation between Sar1 and the membrane bend, α. If we get different sizes of vesicles for different sizes for α we would know that this effect plays a role in the vesicle fission.

Answer

The bottle neck as well as the vesicle scission happen spontaneously because of energy minimization.

The scission of the vesicle could occur because the protein dynamics was updated before the membrane bending model had reached steady state.

When cargo is only applied at a restricted area of the membrane in our model, we expect to have vesicle scission even if the above is true.

The scission might also come from the vesicle having reached a critical size for the given membrane bending, α, in the system.

5.3 Question 3

How does cargo influence the vesicle size?

Increasing the amount of cargo at an ERES accelerates the turnover of Sar1 and decelerates the turnover of Sec [8]. This resulted in the vesicles becoming bigger when the cargo load was increased. This happened both when the cargo load was increased in concentration over the same area, or when the area with cargo is increased while the concentration was fixed. We also saw that vesicles are not produced at all, when the cargo load is too small, either in concentration or spread on the membrane.

Why Vesicles Become Bigger with More Cargo

When we try to understand why the vesicle sizes vary with the amount of cargo, we also need to understand why the vesicles leave the membrane. As I just discussed, this is not completely clear and I will have to assume the reason for vesicle fission when explaining the size dependence.

The fact that the vesicles become bigger with a wider cargo distribution can be understood under the assumption that vesicle fission happens when the spread of Sec catches up with the spread of Sar1. Sec spreads with the same speed as Sar1, though delayed, and will first catch up the Sar1 concentration when Sar1 stops spreading. This happens when the spread of Sar1 reaches particles without cargo. Hence the bigger the cargo area the bigger the vesicle.

The above explanation does not hold when varying cargo concentrations (and fixed width) creates varying vesicle sizes. These results can probably be supported by another explanation for vesicle scission. But to do this we probably have to monitor the velocity of the spread of Sec for different concentrations of cargo.

Without thinking of reasons for vesicle fission it seems biologically plausible that more cargo leads to bigger vesicles and more effective secretion. Both when more cargo means wider spread of cargo or higher concentration.

Answer

The vesicle size increases when the amount of cargo is increased. We observe this both when cargo is increased in concentration or in width.

5.4 Further Research

It would be a major backup for the findings in this thesis if our hypothesis that Sar1 bends the membrane anisotropically can be experimentally verified.

Our suggestion about how to relate isotropic and anisotropic bending to particle shapes could also be further supported. This might be done by looking into crystal structures of the COPII protein or into how Sar1 is inserted into the membrane.

I expect that the vesicle fission in our model could be further investigated by monitoring the velocity and acceleration of the radial spread of Sar1 and Sec. These should be compared to how fast the particles move into the vesicle. This should be compared for different sizes of the time scale separation.

In section 4.8.5 I stated that it should be possible to include the spontaneously formed circular PCP formation into the same simulation as the membrane bending model driven by the COPII protein dynamics, by having a sigmoidal dependence between the membrane bending angle, α, and the Sar1 concentration. This could be tested with new simulations. In that process it could become necessary to optimize the spontaneously formed circular PCP patterns further. This could be done by optimizing the size of the angle between PCP vectors, β, and the size of the area where PCP vectors are applied. Or this optimization could be done by implementing another model modification than β.

In the model in this thesis, the transition from anisotropic bending to isotropic bending happens abruptly when Sec increases above a certain limit. Another way to model the transition could be to have two membrane bending angles: one related to Sar1 that makes anisotropic bending and one related to Sec that makes isotropic bending. This would demand that Sar1 has good adaptation, meaning that the Sar1 concentration goes to zero when inhibited by Sec. This should be possible when $k_1 = 20$.

It could also be further investigated whether the model in this thesis could be modified to produce vesicles outside the typical size range of 60-100 nm, so the vesicles could carry large cargo of several hundred nanometers.

Bibliography

[1] Elisabeth A. Montegna et al. "Sec12 Binds to Sec16 at Transitional ER Sites". In: *PLoS ONE* 7.2 (2012). DOI: https://doi.org/10.1371/journal.pone.0031156.

[2] Meir Aridor et al. "The Sar1 GTPase Coordinates Biosynthetic Cargo Selection with Endoplasmic Reticulum Export Site Assembly". In: *The Journal of Cell Biology* 152.1 (2001), pp. 213–229. DOI: https://doi.org/10.1083/jcb.152.1.213.

[3] Xiping Bi, Richard A. Corpina, and Jonathan Goldberg. "Structure of the Sec23/24–Sar1 pre-budding complex of the COPII vesicle coat". In: *Nature* 419 (2002), pp. 271–277. DOI: https://doi.org/10.1038/nature01040.

[4] Anna Bielli et al. "Regulation of Sar1 NH2 terminus by GTP binding and hydrolysis promotes membrane deformation to control COPII vesicle fission". In: *The Journal of Cell Biology* 171.6 (2005), pp. 919–924. DOI: http://www.jcb.org/cgi/doi/10.1083/jcb.200509095.

[5] Silas Boye Nissen et al. "Theoretical tool bridging cell polarities with development of robust morphologies". In: *eLIFE* 7 (2018). DOI: https://doi.org/10.7554/eLife.38407.

[6] Annika Budnik and David J. Stephens. "ER exit sites – Localization and control of COPII vesicle formation". In: *FEBS Letters* 583 (2009), pp. 3796–3803. DOI: https://doi.org/10.1016/j.febslet.2009.10.038.

[7] Marcus C.S. Lee et al. "Sar1p N-Terminal Helix Initiates Membrane Curvature and Completes the Fission of a COPII Vesicle". In: *Cell* 122 (2005), pp. 605–617. DOI: https://doi.org/10.1016/j.cell.2005.07.025.

[8] Rebecca Forster et al. "Secretory Cargo Regulates the Turnover of COPII Subunits at Single ER Exit Sites". In: *Current Biology* 16 (2006), pp. 173–179. DOI: https://doi.org/10.1016/j.cub.2005.11.076.

[9] Bjarke Frost Nielsen et al. "Model to Link Cell Shape and Polarity with Organogenesis". In: *iScience* 23 (2020). DOI: https://doi.org/10.1016/j.isci.2020.100830.

[10] Michael G. Hanna et al. "Sar1 GTPase Activity Is Regulated by Membrane Curvature". In: *The Journal of Biological Chemistry* 291.3 (2016), pp. 1014–1027. DOI: https://doi.org/10.1074/jbc.M115.672287.

[11] Stephan Heinzer et al. "A model for the self-organization of exit sites in the endoplasmic reticulum". In: *The Journal of Cell Science* 121 (2008), pp. 55–64. DOI: https://doi.org/10.1242/jcs.013383.

[12] Brooke J. Bevis et al. "De novo formation of transitional ER sites and Golgi structures in Pichia pastoris". In: *Nature Publishing Group* 4 (2002), pp. 750–756. DOI: https://doi.org/10.1038/ncb852.

[13] Iris K. Jarsch, Frederic Daste, and Jennifer L. Gallop. "Membrane curvature in cell biology: An integration of molecular mechanisms". In: *Cell Biology* 214.4 (2016), pp. 375–387. DOI: https://doi.org/10.1083/jcb.201604003.

[14] Janine McCaughey and David J. Stephens. "COPII-dependent ER export in animal cells: adaptation and control for diverse cargo". In: *Histochemistry and Cell Biology* 150 (2018), pp. 119–131. DOI: https://doi.org/10.1007/s00418-018-1689-2.

[15] Ehud Meron. "Pattern formation in excitable media". In: *Physics reports* 218.1 (1992), pp. 1–66. DOI: https://doi.org/10.1016/0370-1573(92)90098-K.

[16] Ron Milo and Rob Phillips. *What is the thickness of the cell membrane?* http://book.bionumbers.org/what-is-the-thickness-of-the-cell-membrane/. Last accessed Maj 15, 2021.

[17] Guillermo R. La źaro, Suchetana Mukhopadhyayand, and Micheal F. Hagan. "Why Enveloped Viruses Need Cores — The Contribution of a Nucleocapsid Core to ViralBudding". In: *Biophysical Journal* 114.3 (2018), pp. 619–630. DOI: 10.1016/j.bpj.2017.11.3782.

[18] rhome. *Automatic Differentiation*. https://medium.com/@rhome/automatic-differentiation-26d5a993692b. Last accessed April 29, 2021. 2019.

[19] Mariana Ruiz Villarreal. *Phospholipids aqueous solution structures*. https://commons.wikimedia.org/wiki/File:Phospholipids_aqueous_solution_structures.svg. Last accessed April 29, 2021. 2007.

[20] Juan S. Bonifacino and Benjamin S. Glick. "The Mechanisms of Vesicle Budding and Fusion". In: *Cell* 116 (2004), pp. 153–166. DOI: https://doi.org/10.1016/S0092-8674(03)01079-1.

[21] Kota Saito, Miharu Maeda, and Toshiaki Katada. "IRegulation of the Sar1 GTPase Cycle Is Necessary for Large Cargo Secretion from the Endoplasmic Reticulum". In: *Frontiers in Cell and Developmental Biology* 5.75 (2017). DOI: https://doi.org/10.3389/fcell.2017.00075x.

[22] Joep Sprangers and Catherine Rabouille. "SEC16 in COPII coat dynamics at ER exit sites". In: *Biochemical Society Transactions* 43 (2015), pp. 97–103. DOI: https://doi.org/10.1042/BST20140283.

[23] Yasuyuki Suda, Kazuo Kurokawa, and Akihiko Nakano. "Regulation of ER-Golgi Transport Dynamics by GTPases in Budding Yeast". In: *Frontiers in Cell and Developmental Biology* 5.122 (2018). DOI: https://doi.org/10.3389/fcell.2017.00122.

[24] Thomas Langemark Trojahn. MA thesis. Niels Bohr Institute, p. 66.

[25] Rossella Venditti, Cathal Wilson, and Maria Antonietta De Matteis. "Exiting the ER: what we know and what we don't". In: *Trends in Cell Biology* 24.1 (2014), pp. 9–16. DOI: http://dx.doi.org/10.1016/j.tcb.2013.08.005.

[26] Peter Watson et al. “Sec16 Defines Endoplasmic Reticulum Exit Sites and is Required for Secretory Cargo Export in Mammalian Cells”. In: *Traffic* 7.12 (2006), pp. 1678–1687. DOI: https://doi.org/10.1111/j.1600-0854.2006.00493.x.

[27] Tomohiro Yorimitsu and Ken Sato. “Insights into structural and regulatory roles of Sec16 in COPII vesicle formation at ER exit sites”. In: *MBoC* 23 (2012), pp. 2930–2942. DOI: https://doi.org/10.1091/mbc.e12-05-0356x.

[28] Giulia Zanetti et al. “COPII and the regulation of protein sorting in mammals”. In: *Nature Cell Biology* 14.1 (2012), pp. 20–28. DOI: https://doi.org/10.1016/j.febslet.2009.10.038.

[29] Giulia Zanetti et al. “The structure of the COPII transport-vesicle coat assembled on membranes”. In: *eLife* 2 (2013). DOI: https://doi.org/10.7554/eLife.00951.